Performance Benchmark of Planar Solid Oxide Cells Based on Material Development and Designs

David Udomsilp,* Christian Lenser, Olivier Guillon,* and Norbert H. Menzler*

Solid oxide cell (SOC) technology currently attracts great attention due to its unique potential for substantially contributing to a carbon-neutral power supply. The variety in possible designs and applications—covering oxygen ion and proton conductors and the ability to convert surplus electricity to easily storable synthetic fuels, as well as to produce electricity from these fuels according to demand and availability—provides the excellent position of SOCs with regard to decentralized power generation and distribution. Herein, a reference work on cell performance is provided by highlighting specific advantages of the different cell types, designs, and materials with regard to certain operating conditions, including challenges concerning operational modes, processing, and degradation. In conjunction with a critical examination in terms of relevance and technical feasibility, the data provided enable an assessment of the general potential of the cell types for technology development and connect scientific research to industrial considerations.

1. Introduction

To limit human-made global warming, significant efforts worldwide are dedicated to carbon-neutral power generation and supply as an alternative to fossil-derived energy. Therefore, great interest arises with regard to solid oxide cell (SOC) applications electrochemically converting the chemical energy of liquid or gaseous fuels into electricity and vice versa. The potential of the SOC technology to be a key aspect on the way to carbon-neutrality can be illustrated by the possible impact on the main sectors contributing to global CO_2 emissions. In 2016, only four sectors accounted for 93% of global CO_2 emissions. The largest emitting sector was electricity and heat accounting for 42% of emissions, followed by transport (24%), industry (19%) and buildings (8%).[1] In all of these sectors, SOC-based systems offer the potential to reduce emissions, both through enhanced efficiency and the ability to utilize green fuels. SOC systems are particularly well suited for flexible and decentralized power generation and distribution. In peak periods of renewable power generation from solar or wind, surplus electricity can be converted to synthetic fuels. These fuels can be efficiently stored and easily transported and reconverted to electricity and heat during peak load times or periods of limited availability of renewable energy sources. In industrial production of e.g., steel or glass, carbon emissions can be significantly reduced using H_2 generated from solid oxide electrolysis instead of using fossil sources for iron reduction or thermal management. In the transport sector, SOC-based range extenders for battery electric vehicles offer increased driving range, fast refueling, and fuel flexibility.[2–4] Moreover, the direct conversion enables superior efficiency compared with combustion-based technologies—especially under partial load—combined with silent operation and low or even zero emissions, depending on the fuel used. In this context, the term SOCs describes oxygen-ion (O^{2-}) conducting cells as well as proton (H^+) conducting cells made from oxide ceramics. Furthermore, it also includes the operation in fuel cell mode (generating electricity) or in electrolysis mode (converting electricity into chemicals). The denotation therefore covers four terms: solid oxide fuel cells and electrolysis cells (SOFCs/SOECs) and proton-conducting fuel cells and electrolysis cells (PCFCs/PCECs).

Various SOC concepts were developed and several of them are commercially available or close to market entry.[5–12] The concepts differ in the species acting as charge carrier through the electrolyte, geometrical cell design, and mechanically supporting structure. First substantial progress was achieved by Westinghouse on tubular cells.[13–15] Advantageous properties of the tubular design are a well-supporting structure and a sealing area outside of the heated zone. Nowadays, the majority of concepts utilizes the planar cell design, as volumetric as well as gravimetric power density are typically higher and automation of the processing is easier enabling cheaper fabrication.[15–17] Recently, significant progress in terms of volumetric power density was reported on microtubular cells.[18] However, even

Dr. D. Udomsilp, Dr. C. Lenser, Prof. O. Guillon, Prof. N. H. Menzler
Institute of Energy and Climate Research
Materials Synthesis and Processing (IEK-1)
Forschungszentrum Jülich GmbH
52425 Jülich, Germany
E-mail: d.udomsilp@fz-juelich.de; o.guillon@fz-juelich.de; n.h.menzler@fz-juelich.de

Prof. O. Guillon
Jülich Aachen Research Alliance: JARA-ENERGY
52425 Jülich, Germany

The ORCID identification number(s) for the author(s) of this article can be found under https://doi.org/10.1002/ente.202001062.

if these results are impressive and show potential for small-sized devices, scale-up is expected to prove challenging, as current collection and interconnection of tubular cells is substantially more complex compared with planar cells. The geometrical cell design, together with the materials of the cell components, roughly predefines parameters for cell operation. A typical line of development comprises the development of an operational cell, followed by enhancement of the cell performance, and subsequent optimization of the durability for long-term operation. General tendencies during the past decades point to lower operating temperature, higher performance, and most recently intensified focus on operation in electrolysis mode. The gathered experience and knowledge of electrochemical processes and degradation phenomena indicate that a single line of development is not expedient for universally meeting the current demands, but that cells must be specifically designed with regard to the intended application. That is the intended temperature of operation, stationary versus mobile application, required power density (or acceptable size and weight of a system), etc.

Evaluation of the performance is a central step to match the goals set and the results achieved. This applies to a single cell as well as to stacks and systems. Even when limiting the comparison of performance to single-cell measurements, there are various factors that need to be considered to assure the significance of the conclusions drawn. These include: 1) gas mixtures, 2) feed rates, 3) temperature, and 4) cell dimensions and active area.

In addition to a higher susceptibility to errors when using cells with small active area, the performance of very small button-cells often is difficult to directly transfer to full-size cells or even to stacks. With regard to practical applicability, manufacturing procedures need to be suitable for scale-up. In the case of stack testing, however, there are many additional influences complicating comparison of cell performance. Different stack designs and materials, less-defined gas supply, quality of contacting, and temperature gradients have a pronounced impact on the power output. As an example, geometry and orientation of the air and fuel flow fields considerably influence thermal management of a stack.[19,20] Co-flow, counter-flow or cross-flow exhibit different properties and can be advantageous according to certain operational modes and fuels (H_2, CH_4, etc.). Similarly, characteristic challenges are connected to system design, setup, and operation. Therefore, the topics of stack development and system integration are beyond the scope of this work as they provide data for separate extensive elaboration.

There are various excellent reviews and books available in the literature covering certain cell types, cell components, materials, manufacturing or mode of operation.[16,17,21–41] These articles provide detailed insights into reaction mechanisms, nanoscale material properties, degradation phenomena, and economics of operation to name just a few. The aim of this article is to present an overview of investigated material combinations and the obtained range of performance of planar SOCs, facilitating the assessment of the general potential of the cell types also for nonexperts. This is based on concise description of the most important material properties and consideration of the influence of fabrication methods and test conditions. The technical feasibility of individual approaches and the state of development are considered, to emphasize especially promising approaches

for systematic, application-oriented and -adapted development. With that, this comprehensive review connects scientific research of materials and design on single-cell level to industrial considerations for future technology development.

2. SOC Processing, Testing, Setups, and Materials

This section will be subdivided into four parts. The first subsection provides a brief introduction to processing methods and their influence on the cell properties, followed by a paragraph on the influence of testing conditions. The subsequent parts are dedicated to the type of material used as the electrolyte, oxygen-ion conductors and proton conductors. The state-of-the-art materials are presented including the materials used for air and fuel electrodes. In addition, examples of advanced processing and alternative materials, their performance and potential are discussed.

2.1. Processing of Planar SOCs

Various methods with different sequences of fabrication of the single components are commonly used for manufacturing of planar SOCs. These include (sequential) tape casting, extrusion, pressing, (thermal) spraying, screen printing, electrophoretic deposition (EPD), or thin-film techniques like sol–gel-based dip and spin coating, physical vapor deposition (PVD), and pulsed laser deposition (PLD).[17] Some advanced processing techniques aim at optimization of certain properties in a defined regime of operating conditions. **Table 1** shows processing methods along with information on the effort (such as time, cost, efficiency, scalability) associated with their use and properties of the fabricated layers. All of the presented technologies have been proven to be suitable to manufacture at least one of the layers of SOCs. However, in the view of industrialization (sequential) tape casting and screen printing have been established as the state-of-the-art processing methods.[42–45] This is due to their flexibility with regard to materials and layer thickness as well as their scalability, aiding mass production at low cost. In contrast, extrusion and pressing are mainly suitable for the fabrication of rather thick substrates. Pressing is frequently used in lab-scale experiments as it is generally available and easily applicable, but does not allow for a continuous fabrication. Spraying methods suffer from moderate efficiency and difficult microstructure adjustment. For example, the fabrication of gas-tight electrolyte layers by atmospheric plasma spraying (APS) poses a challenge, same as providing sufficient open porosity of electrodes.[46] More sophisticated thermal spray processes such as high-velocity oxy-fuel spraying (HVOF) come with substantially higher cost of manufacturing. Thin-film techniques like chemical vapor deposition (CVD), PVD, PLD, and sol–gel-based methods typically provide high-quality layers but exhibit higher cost of fabrication because of increased invest or time consumption. For example, the vapor deposition techniques and PLD are carried out in a vacuum chamber and sol–gel methods usually require multiple coating and thermal treatment steps. Therefore, the application of these methods is a tradeoff between acceptable cost and achievable benefit in performance. Especially

Table 1. Processing methods for fabrication of planar SOC. SOA—state-of-the-art processing method used in industrial scale or well-established in lab scale; "✓"—suitable for fabricating respective layer; "X"—not suitable.

Method	Effort and properties	Thickness (dry layer)	Substrate	Fuel electrode	Electrolyte	Barrier (air side)	Air electrode
Tape casting (single layer)	Scalable	40–800 μm	SOA	SOA	SOA	✓	✓
	Continuous						
	Industrialized						
Sequential tape casting	Same as above	5–800 μm (single layer)	SOA	SOA	SOA	✓ (limited)	✓ (impractical)
	Single-step thermal treatment	250–800 μm (multi-layer)					
Tape casting/ lamination/pressing	Limited scalability	40–800 μm (single layer)	SOA	SOA	SOA	✓ (limited)	✓
	Single-step thermal treatment	250–1500 μm (multi-layer)					
Pressing	Lab-scale method	>1 mm	✓	✓ (limited)	✓ (limited)	✓ (limited)	✓ (limited)
	Easy						
	Low cost						
	No thin films						
Extrusion	Industrialized	>500 μm	✓	✓ (limited)	X	X	X
	High wear						
	Anisotropic aspect ratio and microstructure						
Thermal spraying	Industrialized	20–200 μm	X	✓	✓	✓	✓
	High invest						
	Moderate efficiency						
	Microstructure control challenging						
Wet powder spraying	Industrialized	20–200 μm	X	✓	✓	✓	✓
	Moderate efficiency						
	Microstructure control challenging						
Screen printing	Industrialized	3–150 μm	X	SOA	SOA	SOA	SOA
	Scalable						
	Continuous (possible)						
EPD	Well-known in automotive corrosion protection (but not for ceramics)	<5 μm (single layer)	X	✓	SOA	✓	✓
	Careful suspension control required						
Sol–gel	Time consuming	≈1 μm	X	✓ (impractical)	✓	✓	✓ (impractical)
	Batch processing						
	High quality possible						
PVD	High cost	0.5–2 μm	X	✓	✓	SOA	✓
	High layer quality						
CVD	Very high cost	≪1 μm	X	✓ (impractical)	✓	✓	✓ (impractical)
	Very thin layers						
PLD	High cost; not scalable	<1 μm	X	✓	✓	SOA	✓
	Thin layers						
	Low T process						
ESD	Low T process	5–50 μm	X	✓	✓	✓	✓
	Large active surface						
	Microstructure degradation at high T						
Infiltration of scaffolds	Large active surface	–	X	SOA	X	X	SOA
	Time consuming						
	Microstructure degradation at high T						

ADVANCED
SCIENCE NEWS
www.advancedsciencenews.com

Energy Technology
Generation, Conversion, Storage, Distribution
www.entechnol.de

for the deposition of electrolyte layers, the interplay between the surface to be coated and quality of the thin-film electrolyte is crucial. Very smooth and homogeneous surfaces are required to reliably deposit gas-tight layers.[47,48] Highly active electrode microstructures can be achieved by infiltration of nanoparticles/precursors[26,49] in porous scaffolds previously fabricated by, e.g., tape casting or by advanced processing methods like electrostatic spray deposition (ESD).[50,51] In case of infiltration-based techniques, long-term stability is an issue, as coarsening of the nanoparticles at elevated temperature causes performance degradation due to the loss of active surface area.[26] Yet, infiltration may enable microstructural design beyond traditional sintering-based methods, given a thorough consideration of microstructure evolution during operation. ESD provides increased flexibility with regard to the resulting microstructure,[50] enabling tailored layer properties. As an example, a relatively dense interlayer between the electrolyte and the highly porous active electrode can improve adherence as well as interfacial resistance.[52] Again the influence of high-temperature exposure needs to be evaluated carefully as coarsening may degrade the electrode performance. For more detailed information on processing methods, the reader is referred to the relevant literature.[17,23,41,53–55] What should be emphasized here is that processing predetermines the cell properties. The method itself, in combination with raw materials, their preconditioning, ink/suspension formulation, processing parameters, and subsequent steps like thermal treatments critically affects the microstructure of the functional layers and thus cell performance and durability. Hence, substantial improvements may be achieved solely by the optimization of the fabrication in early stages of development.

2.2. Testing of Single Cells

This section describes impacts of testing procedure to ease comparison of results and underline the importance of testing conditions. The theoretical cell voltage (electromotoric force, EMF) of the oxidation of hydrogen at certain conditions can be calculated using the Nernst equation

$$\text{EMF} \approx \frac{-\Delta G}{nF} = \frac{-\Delta G^0}{nF} + \frac{RT}{nF} \ln\left(\frac{p_{H_2} p_{O_2}^{1/2}}{p_{H_2O}}\right) \tag{1}$$

Accordingly, the cell voltage directly depends on temperature and the partial pressures of the reactants at the electrodes. Hence, operating gas composition and absolute pressure substantially affect the measurement of cell performance. The cell voltage can be used to directly calculate the humidity in the fuel, which is useful to determine the amount of gas leakage in the test setup (through both cell and sealing) when using dry H_2 as fuel. Gas tightness cannot be assessed accurately when using humidified H_2 as fuel.

Gas conversion and flow rate of supplied gases (i.e., fuel utilization) play a dominant role under increasing load. This influence is even more pronounced in case of inhomogeneous gas supply over the electrode area, which therefore should be resolved generally. Moreover, the cell temperature may considerably differ from the furnace set point and can increase substantially under high current load, leading to a hysteresis in the I–V

curve. The accuracy of the temperature measurement depends on the position of measurement as thermocouples can mostly not be placed on the cell directly.

Other important aspects for comparison of cell performance are cell dimensions and contacting of the electrodes during the measurement. Fabrication as well as contacting and gas supply are easier for small button-cells than full-sized cells suitable for stacking. To mimic ideal contacting and avoid influences due to inhomogeneous current distribution, some researchers apply noble-metal contacting pastes. However, these might also manipulate the results in either direction. For example, Ag or Pt nanoparticles exhibit pronounced activity for oxygen reduction and therefore might boost apparent performance of air electrodes.[56] In contrast, sintering of contact paste material can close open porosity of electrode structures, accompanied by hindered gas supply and lower performance. In other words, ideal contacting using all measures (such as noble metal mesh) to avoid influences of the contacting is of particular interest in fundamental scientific research focusing on reaction pathways and their individual steps. The closer applied research moves to industrialization, the more economic boundary conditions call for a solution that serves best in terms of combined cost and performance and the focus shifts to utilization of the cell performance on stack and system level.

The most well-controlled parameters for assessment of cell performance and comparison with other work are usually supplied gases, their pressure and (area specific) flow rate. Small variations in fuel humidification cause significant changes in terms of OCV at low total humidity, but tend to alleviate under load due to gas conversion effects. In contrast, a preset water vapor content of 50% will lead to lower power output over the whole current–voltage range in comparison with (almost) dry fuel conditions, but is relatively insensitive to humidity fluctuations. High flow rates and low fuel utilizations are applied in most single-cell characterizations to evaluate the performance limit of cells. Humidification is often used to assure stable output with little fluctuation but kept low for the same purpose of maximum performance. Recently, Klotz, Weber and Ivers-Tiffée recommended clear guidelines for reliable comparison of cell performance, indicating the cell voltage at a current density of $1\,\text{A cm}^{-2}$ and $pH_2O = 0.6\,\text{atm}$ as a reliable indicator for performance comparison due to the insensitivity of these settings to humidity fluctuations, self-heating, or nonlinearity.[57] Notably, the often-specified maximum power density (MPD) of an SOC is meaningless, as it not only reflects operation parameters that are irrelevant to SOC operation due to the low electrical efficiency at low cell voltages, but is also very sensitive to the testing parameters and the cell geometry.

2.3. Cells Based on Oxygen-Ion Conducting Electrolytes

2.3.1. Structural Design and Nomenclature

Oxygen-ion conducting SOCs are named with regard to the mechanically supporting structure.[16,17] Electrolyte-supported cells (ESCs) are usually fabricated by tape casting and sintering of the electrolyte substrate and subsequent application of the electrodes. The thickness of the electrolyte tape depends on the ionic conductivity and the mechanical stability of the

electrolyte material and typically ranges from 40 to 300 μm. Due to the relatively thick electrolyte, ESCs are predominantly operated in the higher temperature range of 750–900 °C. Moreover, the restricted thermal shock resistance limits their use to stationary applications.

The mechanical support can be provided by either of the electrodes as well. In this case, the electrolyte thickness can be reduced to less than 20 μm enabling operation at lower temperatures of 600–800 °C. Fuel electrode-supported cells represent the state-of-the-art of the electrode-supported design and are generally referred to as anode-supported cells (ASCs) originating from the operation in SOFC mode. ESCs and ASCs are the dominating designs used in SOC development and applications. Accordingly, these represent the cell types of commercially available products shown in **Table 2** together with their nominal performance. Other designs use specific substrate materials differing from the functional materials of the cell. An inert support usually is a ceramic material that provides mechanical stability and sufficient open porosity for gas supply but does not participate in electrochemical or reforming reactions.[58–60] Aforementioned designs are often referred to as fully ceramic setups, even though they comprise a cermet (e.g., Ni/YSZ) structure in the reduced state. However, fabrication and assembly are usually performed in the oxidized, and therefore fully ceramic, state (NiO/YSZ). Moreover, ceramic materials are the main constituents of each layer irrespective of the fabrication/operation status. In contrast, metal-supported cells (MSCs) utilize a porous metal for mechanical support. The intention is to make use of the ductility, superior thermal and electrical conductivity, and easy manufacturability of the metal. At the same time, the thickness of more brittle ceramic or cermet layers can be kept to a minimum. This is especially attractive for use in applications that require cyclic operation and robustness against vibrations or high heating/cooling rates. Challenges arise from corrosion of the metal substrate in humid fuel conditions, interdiffusion between substrate and fuel electrode, and substantially different processing conditions required to avoid oxidation of the metal substrate.

This article focuses on fully ceramic designs. Therefore, the reader is referred to MSC-specific literature for further details[29,32,61] and only selected examples of data on MSCs are presented hereafter.

2.3.2. Electrolytes

A variety of oxygen-ion conducting materials was investigated as SOC electrolyte, establishing fluorite and perovskite-type materials as the state-of-the-art electrolytes. Among these, stabilized zirconia, doped ceria, stabilized bismuth oxides, and substituted lanthanum gallates account for the great majority of conducted experiments.

Zirconia is predominantly used in the partially or fully stabilized state, by substitution of Zr with Y (3YSZ and 8YSZ, respectively) or cosubstitution with Sc and Ce (ScSZ, often simply referred to as scandia stabilized zirconia). YSZ is the material of choice in the temperature range between 700 and 900 °C as it provides sufficient oxygen-ion conductivity and mechanical as well as chemical stability under typical operating conditions. Whereas in terms of single properties YSZ does not exhibit the best performance available, most importantly, it outperforms other materials due to the absence of substantial weaknesses.[16,17] When operating the cell at 600–700 °C, ScSZ is of interest as an alternative to YSZ due to its superior ionic conductivity.[62] However, YSZ is still used in many applications because of the higher price of Sc and issues concerning fabrication and phase stability of ScSZ.[16,34] The largest drawback of zirconia-based electrolytes is their reactivity with Sr (and to a lesser extent La) which are elements present in many high-performance air electrodes. Formation of $SrZrO_3$ and/or $La_2Zr_2O_7$ takes place mainly during high-temperature sintering but was also evidenced after long-term exposure to relevant operating temperatures.[63–68] These zirconate phases are electrically insulating and result in an increased polarization resistance, thus lowering performance of the cell.[69]

Table 2. Performance data of commercially available SOCs. Values provided on company websites or extracted from illustrations. Data of fuel cell materials and Elcogen single-cells derived by linear extrapolation of test results with maximum current density of 0.5 A cm^{-2} (measurement data from Elcogen AS provided by Dr. Sergii Pylypko through personal communication).

Manufacturer	Type	Air electrode	Electrolyte	Fuel electrode	$j_{0.7 V}$ [A cm^{-2}]	T [°C]	Reference
Kerafol	ESC	LSM/ScSZ	YSZ	Ni/YSZ	0.47	850 °C	kerafol.com
		LSM/ScSZ	YSZ	Ni/GDC	0.52		
		LSCF	ScSZ	Ni/GDC	0.88		
SOFCMAN	ESC	Not specified	ScSZ	Not specified	0.76	850 °C	sofc.com.cn
	ASC	LSCF/GDC	YSZ	Ni/YSZ	0.9	700 °C	
					≈ 0.6 (Stack)	750 °C	
Fuel cell materials	ASC	LSC	YSZ	Ni/YSZ	0.65 ± 0.01	600 °C	fuelcellmaterials.com
					1.1 ± 0.05	650 °C	
					1.5 ± 0.1	700 °C	
Elcogen	ASC	LSC	YSZ	Ni/YSZ	0.65 ± 0.01	600 °C	Personal communication
					1.11 ± 0.04	650 °C	
					1.6 ± 0.1	700 °C	
					0.25 @ 0.83 V (Stack)	650 °C	elcogen.com

**ADVANCED
SCIENCE NEWS**
www.advancedsciencenews.com

Energy Technology
Generation, Conversion, Storage, Distribution
www.entechnol.de

Application of diffusion barrier layers (DBLs) is commonly used to prevent or minimize the formation of detrimental reaction phases. The effectiveness of DBLs strongly depends on the processing parameters, final microstructure, and material combination.[34,63–69]

Ceria doped with rare-earth elements like Gd (GDC) or Sm (SDC) is an attractive electrolyte material because of its very high ionic conductivity.[62] However, doped ceria is prone to reduction of Ce^{4+} to Ce^{3+} when subjected to the reducing environments present in SOC fuel gas atmospheres, leading to notable electronic conductivity and performance loss due to internal short circuiting. This issue is typically alleviated by inclusion of a pure ionic conductor to block the short-circuiting current. Apart from that, the compatibility with zirconia and conventional air electrode materials makes doped ceria an excellent choice for application as DBL.[33,34,36]

Er-stabilized Bi_2O_3 (ESB) exhibits a defective fluorite structure and provides exceptional oxygen-ion conductivity at low temperature. However, even stronger reducibility than doped ceria, issues regarding phase stability, and reactivity with air electrode materials pose substantial challenges in terms of efficiency and degradation in long-term operation.[33,34,36]

Substituted lanthanum gallate is the most common perovskite-type electrolyte material for SOC and typically applied in a $(La,Sr)(Ga,Mg)O_3$ composition providing high ionic conductivity at intermediate and low operating temperature.[70–73] A significant drawback is a pronounced reactivity with Ni and NiO, which are used in state-of-the-art fuel electrodes.[33,34,36,73]

Table 3 shows the single-cell performance of SOFCs with different electrolytes, fuel electrodes, and air electrode materials. If electrochemical full-cell tests are not available, polarization resistance of the electrode materials derived from symmetrical cell measurements is presented. Presented data are arranged according to the electrolyte materials—LSGM, ESB, stabilized zirconia, and doped ceria—and within these in the order of increasing performance with the best performing material sets shown in bold. As the published values usually represent initial cell performance, long-term stability and degradation behavior has to be kept in mind for evaluation of cell setups. This is another reason why YSZ is mostly chosen as the electrolyte, making use of its high reliability when using compatible electrode materials or suitable diffusion barrier layers.

The configuration with Ni/stabilized zirconia or Ni/doped ceria functional fuel electrode, stabilized zirconia electrolyte, doped ceria barrier layer, and air electrodes made of $(La,Sr)(Co,Fe)O_{3-\delta}$ or composites thereof with doped ceria today is the most common setup of oxygen-ion conducting SOCs including commercial products. Within these, ASCs with Ni/YSZ support and thin-film electrolytes of $\leq10\,\mu m$ thickness provide the highest performance values published. As shown in Table 3, single-cells operating at 700 °C were shown to provide current densities between 2 and 3.4 A cm^{-2} at a cell voltage of 0.7 V when optimizing design and processing, whereas more exotic materials mostly deliver inferior power output. A cross-section of a typical fuel electrode-supported O^{2-}-conducting SOC is shown in **Figure 1**. To point out the difficulty to compare performance data of cells on stack level (compared with single-cell level) the influence of stacking of multiple cells is illustrated by comparing values from previous studies[74–76] in Table 3 as

one example. Whereas nominally identical cells deliver 1.7 A cm^{-2} at 0.7 V and 700 °C in single-cell measurements,[74,75] the current density reaches only 0.9 A cm^{-2} when tested in a stack,[76] as discussed in the Outlook to commercial application of SOCs. Furthermore, testing of identical cells in single-cell and stack setup and detailed analysis of the results revealed that anode polarization and contact resistance on the air side dominate the overall ASR of stacked cells of common SOCs, with minor contributions of electrolyte and air electrode.[77]

2.3.3. Fuel Electrodes

As mentioned earlier and shown in Table 3, Ni-based cermets are the most common fuel electrode material. In fact, they still are the only available electrodes with proven high performance and durability in full-cells and stacks, despite their moderate redox stability and degradation related to Ni coarsening (especially at high temperature) or Ni depletion (mostly in electrolysis mode). Ni/YSZ cermets are well-known and widely applied in SOCs. Replacing YSZ by doped ceria (GDC, SDC) aims at enhancement of catalytic activity, redox stability, and tolerance against carbon deposition and sulfur poisoning.[33,78–83] Formation of secondary phases with poor ionic conductivity and pores at the interface between electrolyte and fuel electrode during high-temperature sintering (>1300 °C) impedes extensive application of ceria-based cermets in combination with stabilized zirconia electrolytes,[84] and necessitates the use of an additional ceria barrier layer between electrolyte and fuel electrode.

Investigation of fully ceramic fuel electrodes aims at development of redox tolerant cells which are less prone to poisoning by fuel impurities. In the current status of research, fully ceramic fuel electrode materials such as substituted Sr-titanates do not reach the high performance achieved with Ni-based cermets. So far, highest performance values obtained are in the range of <1 A cm^{-2} at 700 °C (see the studies by Burnat and coworkers[85–90] in Table 3) corresponding to about 50% of state-of-the-art cermets. If the performance can be enhanced to comparable levels, however, this approach shows great potential to significantly improve durability.[78,80,85,90,91] One of the hot topics in SOC research is the development of electrode materials which favor exsolution of metal nanoparticles from a ceramic host matrix under reducing conditions in the fuel compartment. These embedded nanoparticles are expected to provide large active surface promoting the electrochemical reaction, at the same time being stable against agglomeration as they are pinned to the ceramic matrix.[92–94] A significant benefit is envisaged from successful implementation of such materials, as they combine the high activity of the metal surface with the superior microstructural and redox stability of ceramics.[39,95–100] Application in full-cells and verification of sufficient stability during multiple redox-cycles including exsolution and reincorporation of the metal phase need to be addressed in further research.

2.3.4. Air Electrodes

The area of materials used as air electrode for O^{2-}-conducting SOCs is more diverse. Perovskite type materials of the formula

Table 3. Fuel cell performance of oxygen-ion conducting cells (SOFCs) with different electrolyte, fuel electrode, and air electrode materials in single-cell measurements (unless noted otherwise). "–" indicates measurement of one electrode in a symmetrical cell setup. Best performing material sets are indicated in bold font for each type of electrolyte.

Air electrode	Electrolyte – barrier layer	Fuel electrode	600 °C		700 °C		Remarks	Ref.
			$j_{0.7\,V}$ [A cm^{-2}]	R_P [Ω cm^2]	$j_{0.7\,V}$ [A cm^{-2}]	R_P [Ω cm^2]		
SrCo$_{0.8}$Fe$_{0.2}$O$_3$	LSGM	(Sr/Ba)$_2$FeMoO$_6$			0.4–0.5	2.5–3.1	Ceramic anode	[86]
SrCo$_{0.95}$Mo$_{0.05}$O$_3$	**LSGM**	**Ni/SDC**			**0.5**	**0.07**		[183]
SrCo$_{1.5}$Mo$_{0.5}$O$_6$	**LSGM**	**Ni/SDC**			**0.5**	**0.08**		[184]
SrCo$_{0.8}$Fe$_{0.2}$O$_3$	**LSGM**	**Sr$_2$MgMoO$_6$**			**0.9 (750 °C)**		**Ceramic anode**	[87]
LSM/ESB	ESB	–		0.4				[185]
Pr$_{0.5}$Ba$_{0.5}$MnO$_3$/ESB	**Sm$_{0.075}$Nd$_{0.075}$Ce$_{0.85}$O$_2$/ESB**	**Ni/Sm$_{0.075}$Nd$_{0.075}$Ce$_{0.85}$O$_2$**	**0.7**					[186]
LSM/ESB	YSZ-GDC	Ni/YSZ	0.5 (650 °C)	0.23 (650 °C)			sintering additive CuO	[104]
LSCF	YSZ-GDC	La$_{0.2}$Sr$_{0.8}$Ti$_{0.9}$Ni$_{0.1}$O$_3$/YSZ	0.1 (650 °C)				MSC, exsolution	[95]
LSM/YSZ	YSZ	La$_{0.2}$Sr$_{0.7}$TiO$_3$/GDC			0.5		Ceramic anode, T not specified	[85]
SrFeO$_3$	YSZ-SDC	Ni/YSZ	0.25	0.88	0.65			[187]
SrFeO$_{2.95}$F$_{0.05}$	YSZ-SDC	Ni/YSZ	0.3	0.39	1.0			
SrFeO$_{2.9}$F$_{0.1}$	YSZ-SDC	Ni/YSZ	0.3	0.49	0.9			
Pr$_4$Ni$_3$O$_{10+\delta}$	YSZ-GDC	Ni/YSZ		0.16 (ASR)	0.64	0.025 (ASR)		[124]
LSCF	GDC-YSZ-GDC	Pr$_{0.5}$Ba$_{0.5}$Mn$_{0.9}$Mo$_{0.1}$O$_3$			0.7 (800 °C)		Ceramic anode 800 °C	[89]
LSM/YSZ	YSZ	Ni/YSZ			0.7			[74]
Sr$_2$Fe$_{1.45}$Sc$_{0.05}$Mo$_{0.5}$O$_6$	YSZ-SDC	Ni/YSZ			0.75	0.35		[188]
LSC	ScYSZ-GDC	Ni/GDC infiltrated (La,Sr)(Fe,Ni,Ti)O$_3$-ScYSZ-Fe22Cr	0.6 (650 °C)	0.35 (650 °C)	0.9		MSC exsolution infiltrated	[189]
GDC infiltrated La$_{0.97}$Ni$_{0.5}$Co$_{0.5}$O$_3$	YSZ-GDC	Ni/YSZ			0.9	0.08	50% H$_2$O	[190]
PrBa$_{0.7}$Ca$_{0.3}$Co$_2$O$_5$	YSZ-GDC	Ni/YSZ	0.4	0.16	1.1	0.035		[191]
SrCo$_{0.8}$Fe$_{0.1}$Ga$_{0.1}$O$_3$	YSZ-GDC	Ni/YSZ	0.5		1.3			[192]
BaFe$_{0.95}$Sn$_{0.05}$O$_3$	YSZ-SDC	Ni/YSZ	0.6		1.2	0.03	Co free	[193]
PrBaCo$_{2-x}$O$_{6-\delta}$	YSZ-GDC	Ni/YSZ	0.7	0.2	1 (650 °C)	0.059		[194]
LaNi$_{0.5}$Co$_{0.5}$O$_3$-GDC-YSZ	YSZ	Ni/YSZ		0.07–0.31	1.2	0.02 (air electr.)	rSOC	[195]
(PrLaBa)(FeZn)O$_5$/ SDC	YSZ-GDC	Ni/YSZ	0.7	0.6	1.2	0.1		[196]
LSC	YSZ-GDC	Ni/YSZ	0.7	0.5			PLD AACVD	[197]
LSM/YSZ	YSZ	Ni/YSZ			1.5 (750 °C)			[105]
Sm$_{0.5}$Sr$_{0.5}$CoO$_3$/SDC	YSZ-GDC	Ni/YSZ			1.6			[198]
LSCF	YSZ-GDC	Ni/YSZ	0.6	1.4	1.7	0.25	10 µm YSZ	[74,75]
LSCF	YSZ-GDC	Ni/YSZ	0.3		0.9	< 0.17	Stack	[76]
La$_{0.6}$Ba$_{0.4}$CoO$_3$	YSZ	–	0.17 (R_{surf})				PLD high TEC	[199]
LSC	YSZ	–	0.5				PLD	
(Bi,Sr)(Fe,Nb)O$_3$	YSZ-GDC	Ni/YSZ	0.8	0.16	2	0.04		[115]
La$_{0.65}$Ca$_{0.35}$FeO$_{3-\delta}$	**YSZ-GDC**	**Ni/YSZ**	**0.6**	**0.65**	**2.1**	**0.21**	**3 µm YSZ**	[120]
LSC	**YSZ-GDC**	**Ni/YSZ**	**0.8**		**2.1**		**10 µm YSZ**	[74]
LSCF	**YSZ-GDC**	**Ni/YSZ**	**1.0**	**1.4**	**2.1**	**0.25**	**1 µm YSZ**	[74,75]
BaCo$_{0.4}$Fe$_{0.4}$Zr$_{0.1}$Y$_{0.1}$O$_3$	**YSZ-GDC**	**Ni/YSZ**			**2.3**	**0.31**		[200]
Infiltrated GDC + La$_{0.95}$Co$_{0.4}$Ni$_{0.6}$O$_3$	**YSZ (dense/porous)**	**–**		**0.05**			**Low R_P in symm. cell**	[201]

Table 3. Continued.

Air electrode	Electrolyte – barrier layer	Fuel electrode	600 °C		700 °C		Remarks	Ref.
			$j_{0.7\,V}$ [A cm^{-2}]	R_p [Ω cm^2]	$j_{0.7\,V}$ [A cm^{-2}]	R_p [Ω cm^2]		
LSC	**YSZ-GDC**	**Ni/YSZ**	1.77				**PLD**	[108]
LSC	**YSZ-GDC**	**Ni/YSZ**	1.9		3.4		**1 μm YSZ**	[74,75]
LSC/GDC	**YSZ-GDC**	**Ni/YSZ**	2.0	0.27	2.5 (650 °C)	0.19 (650 °C)	**PLD**	[202]
LSCF	GDC-YSZ-GDC	Ni/GDC	0.53 (0.75 V)				MSC	[203]
LSC	ScYSZ-GDC	Ni/GDC infiltrated Ni22Cr/YSZ			1.44		MSC	[107]
LSCF	YSZ-GDC	Ni/GDC			1.6		MSC	[204]
Pr_6O_{11} infiltrated ScSZ	**ScSZ**	**Ni/SDC infiltrated ScSZ**			2.2		**MSC**	[205]
LSC	**YSZ-GDC**	**Ni/GDC**			3.6		**MSC**	[109]
LSM/ScSZ	ScSZ	$Gd_{0.1}Ce_{0.8}Ni_{0.1}/La_{0.1}Sr_{0.9}Ti_{0.9}Ni_{0.1}O_3$			0.25 (800 °C)		Exsolution	[98]
LSM/ScSZ	ScSZ	$ScSZ/\ La_{0.1}Sr_{0.9}TiO_3 + GDC + Ni/Pd$			0.75–0.9 (800 °C)		Ceramic anode	[91]
LSM/YSZ	ScSZ	$La_{0.9}Ca_{0.1}Fe_{0.9}Nb_{0.1}O_{3-\delta}/ScSZ$			0.5		Ceramic anode	[88]
$Cu_{1.4}Mn_{1.6}O_4$	ScSZ	Ni/ScSZ			0.6			[206]
		$La_{0.5}Sr_{0.5}Fe_{0.8}Cu_{0.15}Nb_{0.05}O_3$	ScSZ-SDC					
		$La_{0.5}Sr_{0.5}Fe_{0.8}Cu_{0.15}Nb_{0.05}O_3$			1 (800 °C)	0.16 (800 °C)	Cu exsolution	[99]
$Pr_{0.5}Sr_{0.5}Cu_{0.2}Fe_{0.8}O_3$	ScSZ-SDC	$La_{0.5}Sr_{0.5}Fe_{0.8}Cu_{0.1}Ti_{0.1}O_3$			0.8	0.26	Ceramic anode	[90]
–	SDC	$La_{0.4}Sr_{0.4}Sc_{0.9}Ni_{0.1}O_3/SDC$				0.25	Exsolution	[96]
Infiltrated $CuCo_2O_4$	ScSZ	Not specified			1			[207]
$Sr_{0.95}Co_{0.7}Nb_{0.1}Fe_{0.2}O_3$	SDC	Ni/SDC	0.05	0.43	0.1	0.11		[208]
$La_2NiO_{4+\delta}$	GDC	–		0.42		0.08	ESD	[122]
$La_3Ni_2O_7/GDC$	GDC	–		0.13		0.03		[121]
$NdBa_{0.96}Co_2O_5$	SDC	(Ni,Cu)/SDC			<0.25 (650 °C)	0.3 (650 °C)		[126]
LSCF/GDC	GDC	$Sr_{0.2}Na_{0.8}Nb_{0.9}V_{0.1}O_3/GDC$			0.25 (650 °C)	0.2 (650 °C)	Ni free	[209]
$LaPrNiO_4$	GDC	Ni/YSZ	0.25	0.12	0.5		ESD	[123]
LSCF/GDC	GDC	Ni/GDC	0.4	0.17				[210]
CuO infiltrated LSCF	SDC	Ni/SDC	0.4					[211]
LSCF/GDC	**GDC**	**–**		0.07			**ESD**	[212]
LSCF	**GDC**	**–**		0.07		0.02 (650 °C)	**ESD**	[52]
$YBa_{0.5}Sr_{0.5}Co_{1.75}Fe_{0.25}O_5/GDC$	**GDC**	**Ni/GDC**	1.5	0.08				[125]
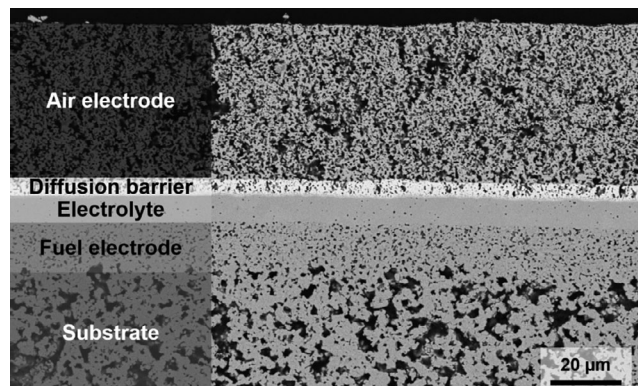
Figure 1. Cross-sectional SEM image of the microstructure of a common fuel electrode-supported SOC with O^{2-}-conducting YSZ electrolyte manufactured at Forschungszentrum Jülich.

ABO_3 represent the state-of-the-art materials. Most extensively studied are lanthanum manganites and lanthanum cobaltites, which are substituted with other elements on the A and/or B site. This substitution is used to improve or adapt material properties like ionic and electronic conductivity, sintering activity, thermal expansion, surface exchange, and reactivity with electrolyte materials and contaminants.[31,101–103] The composites of $La_{1-x}Sr_xMnO_{3-\delta}$ (LSM) and stabilized zirconia used in the early-generation SOCs exhibit compatibility with stabilized zirconia electrolytes but provide moderate performance as the reaction takes place only at triple phase boundaries (see the studies by Blum and coworkers[74,104,105] in Table 3). Nonetheless, LSM/stabilized zirconia compositions are still widely used in ESCs (also see Table 2), as performance is limited by the higher resistance of the electrolyte layer. When aiming at operation below 800 °C, they were largely replaced by mixed ionic electronic conductors (MIEC) such as $La_{1-x}Sr_xCo_{1-y}Fe_yO_{3-\delta}$

**ADVANCED
SCIENCE NEWS**

www.advancedsciencenews.com

Energy Technology
Generation, Conversion, Storage, Distribution

www.entechnol.de

(LSCF), extending the reaction zone to the entire surface of the electrode. Whereas the strontium-substituted lanthanum cobaltite provides the highest electrochemical activity, the addition of Fe improves the material properties with regard to thermal expansion mismatch and stability during processing and cell operation.[17,31,106] High-performance materials such as the Fe-free composition $La_{1-x}Sr_xCoO_{3-\delta}$ (LSC) or $Ba_{1-x}Sr_xCo_{1-y}Fe_yO_{3-\delta}$ (BSCF) enhance electrochemical performance (see the studies by Blum and coworkers[74,75,107–109]) but exhibit significantly larger coefficients of thermal expansion (CTEs) and pronounced chemical expansion increasing the expansion mismatch between electrode and electrolyte.[110–113] Hence the benefit of superior electrochemical performance has to be evaluated in consideration of inferior thermo-chemo-mechanical durability. As the sites in the perovskite lattice can be occupied by various elements, there is a large number of possible element combinations and stoichiometries. In addition to improving performance, substitution or addition of elements is frequently carried out to reduce degradation phenomena. Sr tends to segregate and react with other elements. Therefore, replacing Sr is expected to improve compatibility to stabilized zirconia as well as tolerance against volatile Cr species originating from steel surfaces of interconnectors and Balance-of-Plant (BoP) or S contaminants of the supplied air.[40,114] Segregation of Co is considered less critical, but substitution of Co might contribute to lower cost of SOCs, underlining the interest in Co-free materials.[115–117] Whereas the reported performance of many Sr- or Co-free air electrodes is inferior compared with state-of-the-art materials, $(La,Ca)FeO_{3-\delta}$ was found to provide fast oxygen exchange[118,119] and most recently also high performance in single-cell measurements,[120] as shown in Table 3.

Some other perovskite types and structurally related materials have been attracting attention due to enhanced surface exchange or oxygen-ion transport properties, smaller CTE mismatch, and increased tolerance against Cr species. These include the Sr-free lanthanum nickelates $LaNiO_3$ and La_2NiO_4 as well as further layered perovskites of the Ruddlesden–Popper series $A_{n+1}B_nX_{3n+1}$.[31] The polarization resistances of 0.1–0.4 $\Omega\,cm^2$ obtained at 600 °C (see the studies by Sharma et al.,[121–124] Table 3) are comparable with state-of-the-art LSCF electrodes.[121–124] However, high performance was not yet demonstrated in single-cell tests. Promising performance of 1.5 A cm^{-2} at 0.7 V and 600 °C was reported using a composite of double perovskite $YBa_{0.5}Sr_{0.5}Co_{1.75}Fe_{0.25}O_5$ and GDC as air electrode with GDC electrolyte and Ni/GDC fuel electrode.[125] Double perovskites of the composition $LnA'B_2O_{5+\delta}$ (Ln = La, Pr, Nd, Sm, Gd; A' = Ba, Sr; and B = Co, Fe, Mn) exhibit layer sequences of $A'O—BO_2—LnO_\delta—BO_2$ which feature fast in-plane conductivity of oxygen ions in the Ln^{3+} layers.[125,126]

Dual-phase composites of an active air electrode material and electrolyte phase aim at adaptation of the CTE and/or enhancement of the ionic conductivity in the electrode. Doped ceria is commonly used as the second phase due to its compatibility with most air electrode materials. In addition to the intrinsic material properties like CTE and ionic conductivity, the addition of a second phase can further change electrode properties. The sintering activity of a dual-phase composite differs from a single-phase material. For example by the inhibition of particle coarsening, ceria particles affect the electrode microstructure,

which fundamentally influences the electrochemical properties. Furthermore, the surface properties may change considerably due to scavenging of impurities by one of the compounds, providing a clean and highly active surface of the second phase.[31,127–130] As a consequence, doped ceria that is generally not considered as an active material for oxygen reduction, can improve properties of air electrodes by modifying sintering behavior, microstructure, and bonding to the electrolyte. It should be noted that these implications are not universally valid but strongly depend on material combination, processing, operating conditions, and other characteristics of individual setups.

2.3.5. Solid Oxide Electrolysis Cells

Data of investigations in electrolysis mode is sparse in comparison with fuel cell mode, as shown in **Table 4**. Electrolysis is considered increasingly important driven by economic and environmental issues. Countries that have limited access to fossil resources like Japan or South-Korea push the development of a hydrogen society to become more independent in terms of energy supply. At the same time, large efforts are placed on a climate-neutral economy as specified in the Paris Agreement and the European Green Deal of the EU.[131,132] Therefore, performance and degradation phenomena of cells operated in SOEC mode, have been investigated in more detail recently. The materials used for fabrication of the functional layers are similar to traditional SOFC materials as these exhibit catalytic activity in both operational modes and often provide initial SOEC performance in agreement with SOFC tests. However, comparison of the available data is complicated by a lack of standardized operation conditions. The operating temperature in electrolysis mode is mostly between 700 and 850 °C, which is higher than the average fuel-cell-operating temperature. The operation can be categorized in pure H_2O electrolysis, pure CO_2 electrolysis, and coelectrolysis of H_2O and CO_2.[25,133] Furthermore, the H_2/H_2O ratio of the fuel composition differs in literature due to different amounts of H_2 fed. This can be because of limitations of the experimental setups or to ensure a sufficiently reducing atmosphere. Published data also differ in the cell voltage or current density used for comparison of performance. Most applications aim at operation close to the thermo-neutral point, resulting in a cell voltage around 1.3 V. At this operating point, the net reaction heat and Joule heating of the cell level out, minimizing the required external heating or cooling.[25]

Whereas the initial performance of SOEC mostly is in accordance with SOFC performance, degradation was found to be substantially different when cells are operated in electrolysis mode. In addition to well-known degradation caused by fuel impurities or contaminants, SOEC-specific degradation phenomena occur. Among these, crack formation in the electrolyte or at the electrolyte/air electrode interface, Ni migration leading to depletion of Ni at the electrolyte/fuel electrode interface, and carbon deposition at the fuel electrode when operating on carbon-containing fuel are considered most critical. High current densities and increased polarizations of electrodes and interfaces at higher cell voltage increase degradation rates. Furthermore, the redox reactions at the air and fuel electrode are reversed in comparison with fuel cell operation, which might affect the degree of degradation

Table 4. Electrolysis performance of oxygen-ion conducting cells (SOECs) with different electrolyte, fuel electrode, and air electrode materials in single-cell measurements (unless noted otherwise). Best performing material sets are indicated in bold font.

Air electrode	Electrolyte—barrier layer	Fuel electrode	700 °C		800 °C		Remarks	Ref.
			j [A cm^{-2}]	R_P [Ω cm²]	j [A cm^{-2}]	R_P [Ω cm²]		
La$_{0.6}$Sr$_{0.4}$Fe$_{0.8}$Mn$_{0.2}$O$_3$	LSGM	Ba$_{0.6}$La$_{0.4}$CoO$_3$			0.52 @ 1.6 V (900 °C)			[213]
Ni, Cu, Ni/Cu infiltrated La$_{0.75}$Sr$_{0.25}$Cr$_{0.5}$Mn$_{0.5}$O$_3$/SDC	LSGM	LSM/SDC			0.28 @ 1.2 V (CO$_2$)	0.75–3		[214]
Bi$_{0.42}$Y$_{0.58}$O$_{1.5}$/LSM	YSZ	Ni/YSZ		0.25				[215]
–	YSZ dense/porous	LSM				0.5		[134]
LSC/GDC	**YSZ-GDC**	**Ni/YSZ**		0.15 (750 °C)				[135]
La$_{0.8}$Sr$_{0.2}$Co$_{0.8}$Ni$_{0.2}$O$_3$ infiltrated LSM/GDC	**YSZ**	**Ni/YSZ**			0.8 @ 1.2 V	0.12		[216]
LSC infiltrated LSCF	**YSZ-GDC**	**Ni/YSZ**			0.7 @ 1.1 V	0.06		[137]
LSC infiltrated GDC	**YSZ-GDC**	**Ni/YSZ**	0.3 @ 1.1 V	0.18	0.8 @ 1.1 V	0.09		[217]
LSCF	**YSZ-GDC**	**Ni/YSZ**	0.3 @ 1.1 V	<0.17	0.75 @ 1.1 V	<0.1	Stack	[76]
LSC/GDC	**YSZ-GDC**	**Ni/YSZ**			1 @ 1.1 V	0.14		[147]
Pr$_6$O$_{11}$ infiltrated ScSZ	**ScSZ**	**Ni/SDC infiltrated ScSZ**	1.0 @ 1.1 V		2.4 @ 1.1 V		MSC	[218]

processes. Crack formation on the air side is hypothesized to occur due to high vapor pressure of oxygen in the electrolyte or at the interface to the electrode. Materials and microstructures with improved transport properties and fast oxygen evolution are desired to improve durability. Improved long-term stability was achieved by interface engineering[134] and optimization of the electrode microstructure and composition.[135–137] Carbon deposition can be mitigated by monitoring the gas composition and ensuring sufficient water vapor content.[138] Moreover, new materials are investigated that are less prone to carbon deposition than pure Ni. Examples are Ni–Sn[139] and Ni–Cu alloys or incorporation of Mo in the fuel electrode structure.[140] However, the addition of foreign elements frequently decreases cell performance and processing is complicated due to the low melting point of the alloying elements and limited solubility at high temperature.[140–142]

A deeper understanding of Ni migration is crucial for further SOEC development. Early hypotheses regarding the mechanism of Ni migration were based on evaporation of Ni species in highly humid atmospheres.[143] However, Ni migration does not occur under OCV conditions which present the highest humidity but only under polarization.[144] Comparison of stack test data[145,146] and FactSage calculations of the vapor pressure of Ni species at 800 °C in a typical 90% H$_2$O, 10% H$_2$ atmosphere indicate that evaporation is unlikely to be the sole reason for Ni migration. Ni(OH)$_2$ exhibits the highest vapor pressure of 1.8×10^{-10} bar. Considering 18 000 h of stack operation and the amount of gas fed to the fuel electrode, only 0.25% of the Ni in the functional layer can be evaporated. Therefore, polarization-dependent properties of the fuel electrode cermet are expected to play a key role in Ni migration. This is in agreement with published results indicating enhanced durability achieved by minimization of the electrode overpotential due to optimized processing[147] and observation of polarization-dependent wettability of Ni in contact with YSZ.[148,149] Based on these findings, Trini et al.[150] hypothesized that the reverse effect of Ni loss due to migration

observed during electrolysis operation is likely to occur after very long operation in fuel cell mode, leading to Ni enrichment in the fuel electrode. This assumption was recently supported in a publication of Menzler et al. on the results of the post-test analysis of an SOFC stack operated for 100.000 h at 700 °C.[151]

2.4. Cells based on Proton Conducting Electrolytes

Proton-conducting materials exhibit promising properties for use as SOC electrolyte. Proton conduction is comparably fast at low and intermediate temperatures of 350–550 °C, making PCFCs attractive for low-temperature operation. Moreover, very high fuel utilization and operation at peak power are possible as water is formed at the air side and the fuel is not diluted by water vapor, maintaining safe conditions for redox prone fuel electrodes. However, achieving sufficient conductivity in the range of 10^{-2} S cm^{-1} is challenging at temperatures above 500 °C as dehydration of the material leads to decrease of the charge carrier concentration.

2.4.1. Electrolytes

Acceptor-doped BaZrO$_3$–BaCeO$_3$ solid solutions are the basis for most PCFC electrolytes. Barium zirconate exhibits high phase stability and chemical stability in typical SOC fuel atmospheres containing H$_2$O, CO$_2$, CO, CH$_4$, and H$_2$S but shows limited proton conductivity due to pronounced blocking effects of grain boundaries.[152] In contrast, barium cerates provide very high conductivity, a coarser microstructure with fewer grain boundaries, and high charge carrier concentration but insufficient thermochemical stability during operation. The higher reducibility of BaCeO$_3$ compared with BaZrO$_3$ and reactivity with CO$_2$ and H$_2$O to form carbonates or hydroxides prevent the use of pure BaCeO$_3$ as electrolyte for proton-conducting SOC. The combination of both systems provides an electrolyte material with high conductivity and sufficient stability.[152,153] Y is the most common

dopant and frequently combined with Yb doping to enhance conductivity and catalytic reforming of hydrocarbons. The resulting $Ba(Zr,Ce,Y,Yb)O_{3-\delta}$ (BZCYYb) electrolyte compositions exhibit conductivities in the range of $10^{-2}\,S\,cm^{-1}$ at $600\,°C$ and improved coking resistance.[154,155] Nonetheless, stability in atmospheres containing water vapor, CO_2 or hydrocarbons remains an issue.[153,156] Densification of the electrolyte layer is often reported to present another difficulty. Very high temperatures of $>1600\,°C$ required for densification of single-phase $BaZrO_3$ compositions are in conflict with the requirement of high porosity of electrode substrates, and cause loss of Ba due to evaporation, negatively affecting the proton conductivity. A widespread approach to densify $BaZrO_3$–$BaCeO_3$ mixtures at lower sintering temperature is the addition of suitable amounts of sintering aids such as CuO, NiO, ZnO, and Bi_2O_3 while keeping high proton conductivity.[153] However, it was recently reported that cosintering of the electrolyte on an electrode substrate can promote densification and provide sufficiently dense electrolyte layers even at temperatures as low as $1350\,°C$.[157] This phenomenon is actually not novel but well-known from fabrication of SOFC (YSZ electrolyte on Ni/YSZ substrate). The higher shrinkage of the support presents an additional driving force for electrolyte sintering due to compressive stresses, thereby enhancing densification.[158,159]

Other materials investigated as PCFC electrolyte suffer from insufficient proton conductivity at relevant operating temperature. Lanthanum tungstate presents an alternative to the $Ba(Zr,Ce,Y,Yb)O_{3-\delta}$ materials if very thin films of about $1\,\mu m$ thickness can be manufactured. High thermochemical stability, better sinterability, and less blocking effects of the grain boundaries are advantageous for application as electrolyte, whereas the conductivity is about one order of magnitude lower than the one of $BaZrO_3$–$BaCeO_3$ compositions at $800\,°C$.[160–162]

2.4.2. Fuel Electrodes

Similar to cells based on oxygen-ion conductors, PCFC fuel electrodes are usually cermets made of electrolyte material and NiO, which is reduced to metallic Ni when subjected to fuel conditions at the beginning of operation.[163,164] The microstructure of a representative fuel electrode-supported PCFC is shown in **Figure 2**. Symmetrical cells using other materials such as $BaFeMo_2O_6$ as
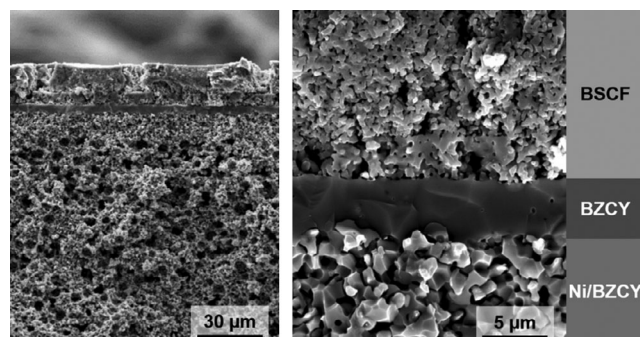
Figure 2. Cross-sectional SEM image of the microstructure of a high-performance fuel electrode-supported proton conducting cell. Adapted with permission.[157] Copyright 2018, Springer Nature.

fuel electrode did not yet achieve performance comparable with Ni/electrolyte cermets.[165]

2.4.3. Air Electrodes

Air electrode materials used for SOFCs are widely applied also as PCFC air electrode and frequently mixed with electrolyte material to form a dual-phase electrode. Addition of the electrolyte phase improves the proton conductivity and extends the available reaction zone, similar to early LSM/YSZ air electrodes for SOFC.[166–168] The pronounced MIEC properties and fast surface exchange are beneficial for both SOFC and PCFC. However, state-of-the-art SOFC air electrodes like LSCF show negligible proton conductivity at relevant operating temperature[169] and many proton-conducting materials suffer from dehydration at temperatures above $400\,°C$. Therefore, development of air electrode materials with enhanced hydration properties and improved stability of protons at elevated temperature is desired. Of special interest are triple conducting materials (e^-, O^{2-}, H^+) to maximize the reaction zone and active volume of air electrodes.[153,170–172] Proton-conducting air electrode materials usually limit the possible sintering temperature to 800–$1000\,°C$ increasing the risk of delamination due to poor contact with the electrolyte and stresses induced by CTE mismatch.[173] Some of the most promising air electrode materials reported are double-perovskites of the composition $LnA'B_2O_{5+\delta}$ (Ln = La, Pr, Nd, Sm, Gd; A' = Ba, Sr; and B = Co, Fe, Mn).[174,175] **Table 5** shows the performance of various PCFCs reported in literature. Most single-cell measurements show moderate performance of 0.4–$0.6\,A\,cm^{-2}$ at $0.7\,V$ and $600\,°C$.[176–178] Substantial performance enhancement to $1.4\,A\,cm^{-2}$ at $0.7\,V$ and $600\,°C$ was achieved using a $PrBa_{0.5}Sr_{0.5}Co_{1.5}Fe_{0.5}O_{5+\delta}$ (PBSCF) air electrode providing enhanced solubility of protons. A dense PBSCF interlayer applied by PVD on the $BaZr_{0.4}Ce_{0.4}Y_{0.1}Yb_{0.1}O_3$ electrolyte is reported to enhance contact between electrode and electrolyte.[170] High performance of $1.75\,A\,cm^{-2}$ was reported using a cell comprising thin ($<5\,\mu m$) BZCY electrolyte fabricated on a co-shrinking Ni/BZCY substrate and BSCF air electrode.[157] Further progress in terms of performance and durability is envisaged by the application of advanced PCFC air electrode materials. Certainly, extended durability (stack) tests are required to evaluate the industrial applicability of PCFCs. Relevant lifetimes cover at least $8000\,h$ (1 year) of operation to become commercially viable, and more likely should last several $10\,000\,h$ in stationary applications. The available single-cell test durations of up to $1400\,h$[156,170,179,180] illustrate the gap in maturity of PCFC technology in comparison with SOFC.

2.4.4. Proton-Conducting Electrolysis Cells

Operation of proton-conducting cells in electrolysis mode (PCEC) was reported to result in substantially lower efficiency than fuel cell operation.[179] Therefore, little data on PCEC are available. Recently, it was shown that BZCYYb compositions show drastically improved PCEC performance due to lower electronic leakage compared with BZY-type materials, reaching between 0.75 and $1.92\,A\,cm^{-2}$ at $1.3\,V$ and $600\,°C$ (3–20%

Table 5. Fuel cell performance of PCFCs with different electrolytes, fuel electrodes, and air electrode materials in single-cell measurements. Best performing material sets are indicated in bold font.

Air electrode	Electrolyte	Fuel electrode	600 °C		700 °C		Remarks	Ref.
			$j_{0.7\,V}$ [A cm^{-2}]	R_p [Ω cm^2]	$j_{0.7\,V}$ [A cm^{-2}]	R_p [Ω cm^2]		
$PrBaCo_2O_5$/Ba(Zr,Ce,Y,Yb)O$_3$ (BZCY)	BZCY $BaZr_{0.3}Ce_{0.5}Y_{0.2}O_3$	Ni/BZCY	P_{max} 0.27 W cm^{-2}		P_{max} 0.67 W cm^{-2}		Bi_2O_3 sintering aid	[219]
$La_3Ni_{1.6}Co_{0.4}O_7$	BZCY	Ni/BZCY	0.3	0.35 (650 °C)	0.5			[220]
LSCF/BZCYYb	BZCYYb	Ni/BZCYYb	0.4		0.5			[221]
$LiNi_{0.8}Co_{0.2}O_2$/BZCY	BZCY	Ni/BZCY	0.5 (650 °C)				ZnO sintering aid	[171]
$(Pr,La)(Ni,Cu,Nb)O_4$ infiltrated BZCY	BZCY	Ni/BZCY	0.4		0.7			[176]
$PrBaCo_2O_5$/BZCYYb	BZCYYb + Co	Ni/BZCYYb	0.4	0.35	0.7	0.12		[222]
$SmBaCo_2O_5$/SDC	$BaCe_{0.8}Y_{0.15}Nd_{0.05}O_3$	$Ni/BaCe_{0.8}Y_{0.15}Nd_{0.05}O_3$	0.4	0.3	0.7	0.08		[177]
$Sm_{0.5}Sr_{0.5}CoO_3$ infiltrated GDC	BZCYYb	Ni/BZCYYb	0.6		0.7			[178]
$BaCo_{0.4}Fe_{0.4}Zr_{0.1}Y_{0.1}O_3$	**BZCYYb**	**Ni/BZCYYb**	**0.9**				**0.6 A cm^{-2} (500 °C)**	[156]
$PrBa_{0.5}Sr_{0.5}Co_{1.5}Fe_{0.5}O_5$	**BZCYYb**	**Ni/BZCYYb**	**1.1**	**0.14**			**Without PLD**	[170]
$PrBa_{0.5}Sr_{0.5}Co_{1.5}Fe_{0.5}O_5$	**BZCYYb**	**Ni/BZCYYb**	**1.4**	**0.14**			**+PLD**	[170]
$Ba_{0.5}Sr_{0.5}Co_{0.8}Fe_{0.2}O_{3-\delta}$	**BZCY**	**Ni/BZCY**	**1.75**	**0.09**			**<5 µm electrolyte 1350 °C sintered**	[157]

Table 6. Electrolysis performance of PCECs with different electrolytes, fuel electrodes, and air electrode materials in single-cell measurements.

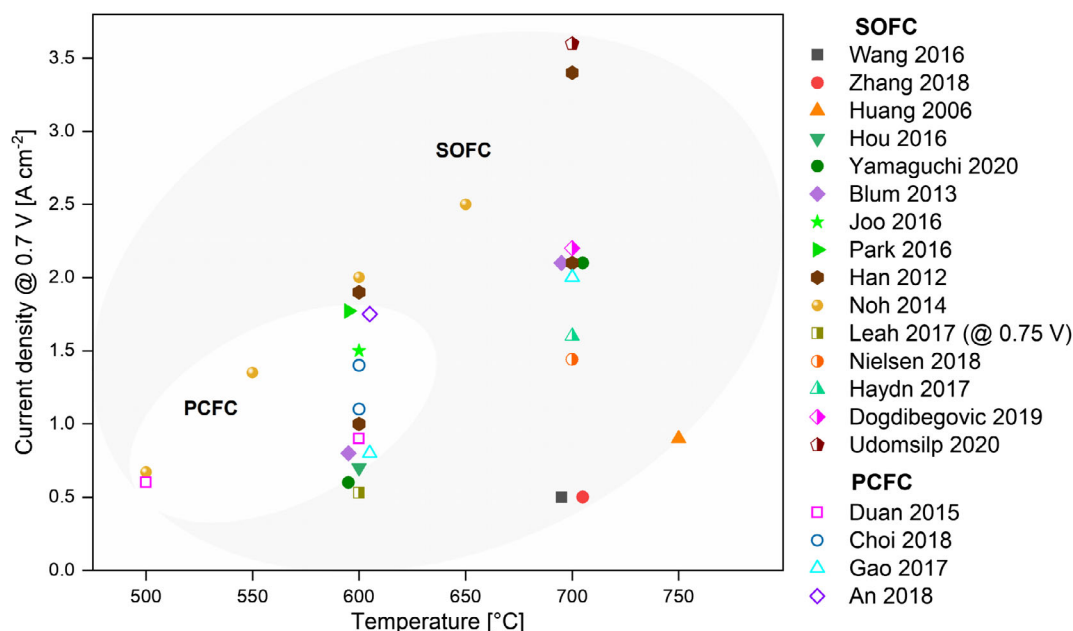| Air electrode	Electrolyte	Fuel electrode	550 °C		600 °C		Remarks	Ref.
			$j_{1.3\,V}$ [A cm^{-2}]	R_p [Ω cm^2]	$j_{1.3\,V}$ [A cm^{-2}]	R_p [Ω cm^2]		
$NdBa_{0.5}Sr_{0.5}Co_{1.5}Fe_{0.5}O_5$/BZCYYb	BZCYYb	Ni/BZCYYb	0.42	0.38	0.75	0.21	"Hybrid"-cell 10% H_2O in H_2 and air; FE not given	[181]
$PrBa_{0.5}Sr_{0.5}Co_{2-x}Fe_xO_5$	BZCYYb	Ni/BZCYYb	0.42		0.85		95Ar/5H$_2$ 12% H_2O in O_2; FE > 97% (500 °C)	[182]
$BaCo_{0.4}Fe_{0.4}Zr_{0.1}Y_{0.1}O_3$	BZCYYb	Ni/BZCYYb	0.75	≈0.17	1.0	≈0.14	10–85% H_2O in N_2; FE > 90%	[179]
$PrBa_{0.5}Sr_{0.5}Co_{1.5}Fe_{0.5}O_5$	BZCYYb	Ni/BZCYYb	0.75	0.25	1.42	0.14	Without PLD; FE 74–87%	[180]
			1.0	0.28	1.92	0.15	+PLD; FE 74–87%	

H_2O),[179–182] as shown in **Table 6**. Despite these improvements, significant contributions of electronic leakage may still reduce the efficiency of electricity to hydrogen conversion. Moreover, the performance in electrolysis mode cannot be directly extracted from the I–V curve, contrary to fuel cell operation. In both operational modes, an internal electronic leakage decreases the cell voltage. In fuel cell mode, this directly corresponds to lower performance. In electrolysis, however, a lower voltage at given current indicates an improved performance assuming constant conversion efficiency. It is therefore important, to include the Faradaic efficiency (FE), which describes the ratio of produced amount of hydrogen to the theoretical amount assuming full conversion. Otherwise, the provided data only describe the power input without indication of product output. Whereas in some works values up to 98% were obtained,[179] others obtained lower FE of 76%.[180]

3. Conclusion

Many novel materials have been investigated for application in SOC. Promising characteristics of these newly developed materials were mainly obtained in symmetrical cell setups, as they enable easy fabrication and testing. However, the validation of high performance in full-cell tests either was not yet addressed or did not provide the intended benefit. In parallel, setups utilizing traditional material combinations were optimized as well, thus still providing the highest power output published (see **Figure 3**). Current densities of 2.0–3.4 A cm^{-2} at 0.7 V and 700 °C are reported for state-of-the-art cells consisting of Ni/YSZ substrate and fuel electrode, YSZ electrolyte, GDC diffusion barrier, and air electrodes made of (La,Sr)(Co,Fe)O$_{3-\delta}$ or dual-phase composites thereof with doped ceria. This emphasizes the importance of microstructure, processing, and combined properties of the applied materials. Whereas 700–800 °C is a quite common range of SOC (ESC/ASC) operating temperature at which traditional materials show beneficial properties, different material combinations, or processing techniques can be advantageous when the intended application and operation conditions change. Especially, for low-temperature operation, highly active electrode structures with large active surface and low interfacial resistance to the electrolyte are crucial. For this, suitable processing needs to be combined with long-term

**ADVANCED
SCIENCE NEWS**
www.advancedsciencenews.com

Energy Technology
Generation, Conversion, Storage, Distribution
www.entechnol.de

Figure 3. Current density of selected SOFC (closed symbols; MSC—half-filled symbols) and PCFC (open symbols) achieved in single-cell tests.

stability at operating temperature. High-temperature exposure should be kept to a minimum to avoid loss of active surface by coarsening. Advanced processing techniques like PVD and PLD can provide high-quality layers with adjustable microstructure providing enhanced performance. However, industrial application is impeded by their higher cost and limited scalability.

Large improvements were achieved with regard to the development of high-performance air electrode materials, which presented the bottleneck in early-stage research. This, in turn, opens the possibility to exploit the potential of enhanced fuel electrodes in further activities. Application of doped ceria in fuel electrodes is of high interest for two reasons. First, the electrochemical activity of ceria under fuel conditions contributes to enhanced cell performance. Second, Ni/doped ceria cermets show potential for increased stability in SOEC mode due to reduced electrode overpotential. An issue to be solved for widespread application of ceria-based fuel electrodes is their processing in contact with a YSZ electrolyte, as interdiffusion leads to pore formation at the interface and increased ohmic resistance. Doped ceria is highly relevant also as an electrolyte material when aiming at low operating temperature. Here, effective measures need to be established to avoid electronic leakage, e.g., by application of blocking layers. If successfully realized, doped ceria electrolytes may contribute substantially to enhanced low-temperature performance.

Great potential is attributed to PCFCs when aiming at low-temperature operation. Very promising properties were identified in early-stage research but considerable improvement is still required to effectively compete with existing SOFC designs. Here, the development of better air electrodes exhibiting adequate proton conductivity at operating temperature is especially important, together with the evaluation of long-term stability ($\gg 1000$ h), scale-up, and stack testing.

In summary, it becomes clear that the choice of cell type, design, materials, and fabrication techniques strongly depends on the intended application. Operating temperature, the fuel to be used, desired lifetime, thermal as well as redox cyclability, and of course cost and performance targets have to be considered to select the optimum cell type. From this, it can be deduced, that the future SOC technology will not be represented by a single state-of-the-art cell covering all sorts of applications, but more likely will consist of customized designs serving particular operating conditions. The data on cell performance, material properties, and manufacturing presented in this article provide a basis for goal-oriented development in academic research as well as a guideline for industrial considerations.

3.1. Outlook to Commercial Application of SOCs.

For successful commercialization of SOCs, the single-cell performance and durability is only the first step of development. As a single cell only provides a voltage of about 1 V, several cells need to be connected to form a stack, meeting industrial requirements with regard to power output. Some fundamental differences and limitations have to be considered when operating SOCs in a stack in comparison with the single-cell characteristics. Reliable mechanical integration, sealing, electrical contact, and gas supply are examples for basic considerations in stack design. All of these factors contribute to losses and affect durability in stack operation to individual extent. Stacking of cells introduces additional interfaces between cells, interconnectors, barrier layers, and contact layers. These interfaces present extra barriers for current flow and therefore cause contact resistances. Another challenge is a homogeneous gas distribution between the layers as well as within each cell. A 3D temperature distribution with a mean stack temperature rather than a homogeneous

temperature at every active site causes different reaction rates, local fuel utilizations, and thermal stresses which complicate stack operation. Furthermore, characterization of small single cells is often performed with rather small fuel utilization, whereas stack operation aims at high fuel utilization to efficiently exploit the chemical energy of the fuel. As a result, cells assembled in a stack generally do not deliver the same power output as an identical cell tested in single-cell operation. To illustrate the magnitude of this issue, recent results show that the current output of a high-performance cell in a Jülich F10 stack is only about 50% of the current measured on identical cells in a single-cell test, at $700\,°C$ and a cell voltage of 0.8 V.

Also, degradation behavior is likely to differ between ideal lab conditions of single-cell testing and real stack operation. This is due to contaminants of fuels (S- or C-containing species) and air (CO_2, H_2O, S, and Cr), different operating conditions, or inhomogeneous gas- and temperature-distribution to name just a few causes. Consequently, the job is not done after the optimization of single materials, but tests in real stacks or stack-mimicking environments (e.g., Cr-containing interconnector material) are crucial parts of material development. Subsequently, stack and system development are another important topic on the way to widespread application of SOCs.

Acknowledgements

Conflict of Interest

The authors declare no conflict of interest.

Author Contributions

Conceptualization: N.H.M. and D.U.; Investigation: D.U., C.L. and N.H.M.; Writing—Original Draft: D.U.; Writing—Review & Editing: C.L., N.H.M., and O.G.; Visualization: D.U.; Supervision: N.H.M.; Project Administration: N.H.M.

Keywords

[1] IEA, CO2 Emissions from Fuel Combustion 2018, https://webstore.iea.org/download/direct/2373?filename=co2_emissions_from_fuel_combustion_2018_highlights.pdf (accessed: July 2019).

[2] V. Lawlor, M. Reissig, J. Makinson, J. Rechberger, *ECS Trans.* **2017**, *78*, 191.

[3] J. Rechberger, M. Reissig, V. Lawlor, *Der Antrieb von morgen 2018*, Springer Fachmedien Wiesbaden, Wiesbaden **2018**, p. 51.

[4] L. Nissan Motors Co., *Press release – range extender*, **2016**, https://newsroom.nissan-global.com/releases/release-3e21870a4078f6ae6a08693da300e19f-160614-01-e?year=2016&month=6 (accessed: September 2017).

[5] A. Ballard, T. Domanski, L. Rees, C. Nobbs, N. Lawrence, K. Heffer, J. Harman, C. Evans, P. Barnard, S. Mukerjee, M. Selby, *ECS Trans.* **2019**, *91*, 117.

[6] C. Geipel, K. Hauptmeier, K. Herbrig, F. Mittmann, M. Münch, M. Pötschke, L. Reichel, T. Strohbach, T. Seidel, A. Surrey, C. Walter, *ECS Trans.* **2019**, *91*, 123.

[7] R. Küngas, P. Blennow, T. Heiredal-Clausen, T. Holt Nørby, J. Rass-Hansen, J. B. Hansen, P. G. Moses, *ECS Trans.* **2019**, *91*, 215.

[8] A. Mai, J. G. Grolig, M. Dold, F. Vandercruysse, R. Denzler, B. Schindler, A. Schuler, *ECS Trans.* **2019**, *91*, 63.

[9] M. Noponen, P. Torri, J. Göös, J. Puranen, H. Kaar, S. Pylypko, M. Roostar, E. Õunpuu, *ECS Trans.* **2019**, *91*, 91.

[10] O. Posdziech, T. Geißler, K. Schwarze, R. Blumentritt, *ECS Trans.* **2019**, *91*, 2537.

[11] D. Hara, *ECS Trans.* **2019**, *91*, 3.

[12] T. Nakao, S. Inoue, S. Uenoyama, Y. Takuwa, M. Suzuki, *ECS Trans.* **2019**, *91*, 43.

[13] R. A. George, *J. Power Sources* **2000**, *86*, 134.

[14] S. C. Singhal, *High Temperature Solid Oxide Fuel Cells: Fundamentals, Design and Applications*, Elsevier, Oxford, **2003**.

[15] S. C. Singhal, *Solid State Ion.* **2002**, *152–153*, 405.

[16] D. J. L. Brett, A. Atkinson, N. P. Brandon, S. J. Skinner, *Chem. Soc. Rev.* **2008**, *37*, 1568.

[17] N. H. Menzler, F. Tietz, S. Uhlenbruck, H. Buchkremer, D. Stöver, *J. Mater. Sci.* **2010**, *45*, 3109.

[18] T. Li, T. M. M. Heenan, M. F. Rabuni, B. Wang, N. M. Farandos, G. H. Kelsall, D. Matras, C. Tan, X. Lu, S. D. M. Jacques, D. J. L. Brett, P. R. Shearing, M. Di Michiel, A. M. Beale, A. Vamvakeros, K. Li, *Nat. Commun.* **2019**, *10*, 1497.

[19] N. Russner, S. Dierickx, A. Weber, R. Reimert, E. Ivers-Tiffée, *J. Power Sources* **2020**, *451*, 227552.

[20] E. Achenbach, *J. Power Sources* **1994**, *49*, 333.

[21] Z. Gao, L. V. Mogni, E. C. Miller, J. G. Railsback, S. A. Barnett, *Energy Environ. Sci.* **2016**, *9*, 1602.

[22] C. Graves, S. D. Ebbesen, M. Mogensen, K. S. Lackner, *Renewable Sustainable Energy Rev.* **2011**, *15*, 1.

[23] O. Guillon, A. Dash, C. Lenser, S. Uhlenbruck, G. Mauer, *Adv. Eng. Mater.* **2020**, *22*, 2000529.

[24] C. M. Harrison, P. R. Slater, R. Steinberger-Wilckens, *Solid State Ion.* **2020**, *354*, 115410.

[25] A. Hauch, R. Küngas, P. Blennow, A. B. Hansen, J. B. Hansen, B. V. Mathiesen, M. B. Mogensen, *Science* **2020**, *370*, eaba6118.

[26] S. P. Jiang, *Mater. Sci. Eng., A* **2006**, *418*, 199.

[27] M. B. Mogensen, M. Chen, H. L. Frandsen, C. Graves, J. B. Hansen, K. V. Hansen, A. Hauch, T. Jacobsen, S. H. Jensen, T. L. Skafte, X. Sun, *Clean Energy* **2019**, *3*, 175.

[28] F. Wang, H. Kishimoto, T. Ishiyama, K. Develos-Bagarinao, K. Yamaji, T. Horita, H. Yokokawa, *J. Power Sources* **2020**, *478*, 228763.

[29] V. V. Krishnan, *Wiley Interdiscip. Rev.: Energy Environ.* **2017**, *6*, e246.

[30] A. B. Stambouli, E. Traversa, *Renewable Sustainable Energy Rev.* **2002**, *6*, 433.

[31] C. Sun, R. Hui, J. Roller, *J. Solid State Electrochem.* **2010**, *14*, 1125.

[32] M. C. Tucker, *J. Power Sources* **2010**, *195*, 4570.

[33] S. P. S. Badwal, F. T. Ciacchi, *Ionics* **2000**, *6*, 1.

[34] J. W. Fergus, *J. Power Sources* **2006**, *162*, 30.

[35] H. Inaba, H. Tagawa, *Solid State Ion.* **1996**, *83*, 1.

[36] V. V. Kharton, F. M. B. Marques, A. Atkinson, *Solid State Ion.* **2004**, *174*, 135.

[37] E. D. Wachsman, K. T. Lee, *Science* **2011**, *334*, 935.

[38] Y. Zhang, R. Knibbe, J. Sunarso, Y. Zhong, W. Zhou, Z. Shao, Z. Zhu, *Adv. Mater.* **2017**, *29*, 1700132.

[39] A. Atkinson, S. Barnett, R. J. Gorte, J. T. S. Irvine, A. J. McEvoy, M. Mogensen, S. C. Singhal, J. Vohs, *Nat. Mater.* **2004**, *3*, 17.

[40] H. Yokokawa, H. Tu, B. Iwanschitz, A. Mai, *J. Power Sources* **2008**, *182*, 400.

[41] J. B. Goodenough, K. Huang, *Solid Oxide Fuel Cell Technology: Principles, Performance and Operations*, Woodhead Publishing, Oxford **2009**.

[42] N. Christiansen, J. B. Hansen, H. Holm-Larsen, M. Juel Jórgensen, M. Wandel, P. Vang Hendriksen, A. Hagen, S. Ramousse, *ECS Trans.* **2009**, *25*, 133.

[43] N. Christiansen, J. B. Hansen, H. H. Larsen, S. Linderoth, P. H. Larsen, P. V. Hendriksen, A. Hagen, *ECS Trans.* **2007**, *7*, 31.

[44] M. Noponen, P. Torri, J. Göös, D. Chade, P. Hallanoro, A. Temmo, A. Koit, E. Ounpuu, *ECS Trans.* **2015**, *68*, 151.

[45] S. Aruliah, S. Amarasinghe, J. Love, R. Ratnaraj, A. Summergreene, M. Watts, *ECS Trans.* **2007**, *7*, 51.

[46] O. Kesler, M. Cuglietta, J. Harris, J. Kuhn, M. Marr, C. Metcalfe, *ECS Trans.* **2013**, *57*, 491.

[47] R. Nédélec, S. Uhlenbruck, D. Sebold, V. A. C. Haanappel, H. P. Buchkremer, D. Stöver, *J. Power Sources* **2012**, *205*, 157.

[48] S. Vieweger, R. Mücke, N. H. Menzler, H. P. Buchkremer, *Fuel Cells* **2013**, *13*, 556.

[49] T. Z. Sholklapper, H. Kurokawa, C. P. Jacobson, S. J. Visco, L. C. De Jonghe, *Nano Lett.* **2007**, *7*, 2136.

[50] C. H. Chen, M. H. J. Emond, E. M. Kelder, B. Meester, J. Schoonman, *J. Aerosol Sci.* **1999**, *30*, 959.

[51] D. Marinha, C. Rossignol, E. Djurado, *J. Solid State Chem.* **2009**, *182*, 1742.

[52] O. Celikbilek, L. Dessemond, E. Djurado, *ECS Trans.* **2017**, *78*, 747.

[53] C. B. Carter, M. G. Norton, *Ceramic Materials [E-Book]: Science and Engineering*, 2nd ed., Springer, New York, NY, **2013**.

[54] M. N. Rahaman, *Ceramic Processing and Sintering*, 2nd ed., CRC Press, Boca Raton, Florida **2003**.

[55] K. Kendall, in *High-Temperature Solid Oxide Fuel Cells for the 21st Century*, 2nd ed., Academic Press, Boston **2016**, p. 25.

[56] Y. Gong, C. Qin, K. Huang, *ECS Electrochem. Lett.* **2012**, *2*, F4.

[57] D. Klotz, A. Weber, E. Ivers-Tiffée, *Electrochim. Acta* **2017**, *227*, 110.

[58] E. Matte, G. Holzlechner, L. Epple, D. Stolten, P. Lupetin, *J. Power Sources* **2019**, *413*, 334.

[59] F. Wankmüller, M. Meffert, N. Russner, A. Weber, J. Schmieg, H. Störmer, T. Dickel, P. Lupetin, N. Maier, D. Gerthsen, E. Ivers-Tiffée, *J. Mater. Sci.* **2020**, *55*, 11120.

[60] F. Grimm, N. H. Menzler, O. Guillon, *J. Power Sources* **2020**, *451*, 227607.

[61] M. Haydn, K. Ortner, T. Franco, S. Uhlenbruck, N. H. Menzler, D. Stöver, G. Bräuer, A. Venskutonis, L. S. Sigl, H.-P. Buchkremer, R. Vaßen, *J. Power Sources* **2014**, *256*, 52.

[62] J. Zhang, C. Lenser, N. H. Menzler, O. Guillon, *Solid State Ion.* **2020**, *344*, 115138.

[63] N. Jordan, W. Assenmacher, S. Uhlenbruck, V. A. C. Haanappel, H. P. Buchkremer, D. Stöver, W. Mader, *Solid State Ion.* **2008**, *179*, 919.

[64] R. Knibbe, J. Hjelm, M. Menon, N. Pryds, M. Søgaard, H. J. Wang, K. Neufeld, *J. Am. Ceram. Soc.* **2010**, *93*, 2877.

[65] H. S. Noh, J. W. Son, H. Lee, J. S. Park, H. W. Lee, J. H. Lee, *Fuel Cells* **2010**, *10*, 1057.

[66] M. Sase, D. Ueno, K. Yashiro, A. Kaimai, T. Kawada, J. Mizusaki, *J. Phys. Chem. Solids* **2005**, *66*, 343.

[67] S. Uhlenbruck, N. Jordan, D. Sebold, H. P. Buchkremer, V. A. C. Haanappel, D. Stöver, *Thin Solid Films* **2007**, *515*, 4053.

[68] S. Uhlenbruck, T. Moskalewicz, N. Jordan, H. J. Penkalla, H. P. Buchkremer, *Solid State Ion.* **2009**, *180*, 418.

[69] J. Szász, F. Wankmüller, V. Wilde, H. Störmer, D. Gerthsen, N. H. Menzler, E. Ivers-Tiffée, *J. Electrochem. Soc.* **2018**, *165*, F898.

[70] T. Ishihara, H. Matsuda, Y. Takita, *J. Am. Chem. Soc.* **1994**, *116*, 3801.

[71] K. Huang, R. S. Tichy, J. B. Goodenough, *J. Am. Ceram. Soc.* **1998**, *81*, 2565.

[72] K. Huang, R. S. Tichy, J. B. Goodenough, *J. Am. Ceram. Soc.* **1998**, *81*, 2576.

[73] K. Huang, R. Tichy, J. B. Goodenough, C. Milliken, *J. Am. Ceram. Soc.* **1998**, *81*, 2581.

[74] L. Blum, L. G. J. de Haart, J. Malzbender, N. H. Menzler, J. Remmel, R. Steinberger-Wilckens, *J. Power Sources* **2013**, *241*, 477.

[75] F. Han, R. Mücke, T. Van Gestel, A. Leonide, N. H. Menzler, H. P. Buchkremer, D. Stöver, *J. Power Sources* **2012**, *218*, 157.

[76] Q. Fang, L. Blum, N. H. Menzler, *J. Electrochem. Soc.* **2015**, *162*, F907.

[77] C. Lenser, J. Zurek, D. Naumenko, C.-A. Thieu, J.-W. Son, U. de Haart, Q. Fang, L. Blum, N. H. Menzler, *J. Power Sources* **2020**, *474*, 228671.

[78] S. P. Jiang, S. H. Chan, *J. Mater. Sci.* **2004**, *39*, 4405.

[79] W. C. Chueh, Y. Hao, W. Jung, S. M. Haile, *Nat. Mater.* **2011**, *11*, 155.

[80] M. Gerstl, A. Hutterer, J. Fleig, M. Bram, A. K. Opitz, *Solid State Ion.* **2016**, *298*, 1.

[81] M. Gerstl, A. Nenning, R. Iskandar, V. Rojek-Wöckner, M. Bram, H. Hutter, A. Opitz, *Materials* **2016**, *9*, 649.

[82] T. Nakamura, K. Yashiro, A. Kaimai, T. Otake, K. Sato, T. Kawada, J. Mizusaki, *J. Electrochem. Soc.* **2008**, *155*, B1244.

[83] V. A. Rojek-Wöckner, A. K. Opitz, M. Brandner, J. Mathé, M. Bram, *J. Power Sources* **2016**, *328*, 65.

[84] C. Lenser, N. H. Menzler, *Solid State Ion.* **2019**, *334*, 70.

[85] D. Burnat, G. Nurk, L. Holzer, M. Kopecki, A. Heel, *J. Power Sources* **2018**, *385*, 62.

[86] Y. Huan, Y. Li, B. Yin, D. Ding, T. Wei, *J. Power Sources* **2017**, *359*, 384.

[87] Y.-H. Huang, R. I. Dass, Z.-L. Xing, J. B. Goodenough, *Science* **2006**, *312*, 254.

[88] X. Kong, X. Zhou, Y. Tian, X. Wu, J. Zhang, W. Zuo, X. Gong, Z. Guo, *J. Power Sources* **2016**, *316*, 224.

[89] Y.-F. Sun, Y.-Q. Zhang, B. Hua, Y. Behnamian, J. Li, S.-H. Cui, J.-H. Li, J.-L. Luo, *J. Power Sources* **2016**, *301*, 237.

[90] Z. Xu, Y.-M. Yin, J. Lu, L. Xu, N. Zhou, J.-W. Yin, Z.-F. Ma, *J. Electrochem. Soc.* **2016**, *163*, F737.

[91] X. Shen, K. Sasaki, *J. Power Sources* **2016**, *320*, 180.

[92] L. De Rogatis, M. Cargnello, V. Gombac, B. Lorenzut, T. Montini, P. Fornasiero, *ChemSusChem* **2010**, *3*, 24.

[93] O. Kwon, S. Sengodan, K. Kim, G. Kim, H. Y. Jeong, J. Shin, Y.-W. Ju, J. W. Han, G. Kim, *Nat. Commun.* **2017**, *8*, 15967.

[94] D. Neagu, G. Tsekouras, D. N. Miller, H. Ménard, J. T. S. Irvine, *Nat. Chem.* **2013**, *5*, 916.

[95] A. M. Dayaghi, K. J. Kim, S. Kim, J. Park, S. J. Kim, B. H. Park, G. M. Choi, *J. Power Sources* **2016**, *324*, 288.

[96] Y. Gao, D. Chen, M. Saccoccio, Z. Lu, F. Ciucci, *Nano Energy* **2016**, *27*, 499.

[97] A. Nenning, L. Volgger, E. Miller, L. V. Mogni, S. Barnett, J. Fleig, *J. Electrochem. Soc.* **2017**, *164*, F364.

[98] X. Shen, T. Chen, S. R. Bishop, N. H. Perry, H. L. Tuller, K. Sasaki, *J. Power Sources* **2017**, *370*, 122.

[99] N. Zhou, Y.-M. Yin, Z. Chen, Y. Song, J. Yin, D. Zhou, Z.-F. Ma, *J. Electrochem. Soc.* **2018**, *165*, F629.

[100] J. T. S. Irvine, D. Neagu, M. C. Verbraeken, C. Chatzichristodoulou, C. Graves, M. B. Mogensen, *Nat. Energy* **2016**, *1*, 15014.

**ADVANCED
SCIENCE NEWS**

www.advancedsciencenews.com

Energy Technology
Generation, Conversion, Storage, Distribution

www.entechnol.de

[101] S. B. Adler, J. A. Lane, B. C. H. Steele, *J. Electrochem. Soc.* **1996**, *143*, 3554.

[102] T. Ishihara, *Perovskite Oxide for Solid Oxide Fuel Cells*, Springer, Dordrecht **2009**.

[103] N. Q. Minh, T. Takahashi, in *Science and Technology of Ceramic Fuel Cells*, Elsevier Science Ltd, Oxford **1995**, p. 117.

[104] S. J. Kim, A. M. Dayaghi, K. J. Kim, G. M. Choi, *J. Power Sources* **2017**, *344*, 218.

[105] H. Shimada, T. Yamaguchi, H. Sumi, K. Nomura, Y. Yamaguchi, Y. Fujishiro, *J. Power Sources* **2017**, *341*, 280.

[106] A. Mai, V. A. C. Haanappel, S. Uhlenbruck, F. Tietz, D. Stöver, *Solid State Ion.* **2005**, *176*, 1341.

[107] J. Nielsen, Å. H. Persson, T. T. Muhl, K. Brodersen, *J. Electrochem. Soc.* **2018**, *165*, F90.

[108] J. H. Park, S. M. Han, K. J. Yoon, H. Kim, J. Hong, B.-K. Kim, J.-H. Lee, J.-W. Son, *J. Power Sources* **2016**, *315*, 324.

[109] D. Udomsilp, J. Rechberger, R. Neubauer, C. Bischof, F. Thaler, W. Schafbauer, N. H. Menzler, L. G. J. de Haart, A. Nenning, A. K. Opitz, O. Guillon, M. Bram, *Cell Rep. Phys. Sci.* **2020**, *1*, 100072.

[110] Z. Shao, S. M. Haile, *Nature* **2004**, *431*, 170.

[111] H. Ullmann, N. Trofimenko, F. Tietz, D. Stöver, A. Ahmad-Khanlou, *Solid State Ion.* **2000**, *138*, 79.

[112] B. Wei, Z. Lü, X. Huang, J. Miao, X. Sha, X. Xin, W. Su, *J. Eur. Ceram. Soc.* **2006**, *26*, 2827.

[113] S. Baumann, W. A. Meulenberg, H. P. Buchkremer, *J. Eur. Ceram. Soc.* **2013**, *33*, 1251.

[114] A. Beez, X. Yin, N. H. Menzler, R. Spatschek, M. Bram, *J. Electrochem. Soc.* **2017**, *164*, F3028.

[115] L. Gao, Q. Li, L. Sun, X. Zhang, L. Huo, H. Zhao, J.-C. Grenier, *J. Power Sources* **2017**, *371*, 86.

[116] N. V. Lyskov, L. M. Kolchina, M. Z. Galin, G. N. Mazo, *Solid State Ion.* **2018**, *319*, 156.

[117] S. Pang, W. Wang, T. Chen, X. Shen, Y. Wang, K. Xu, X. Xi, *J. Power Sources* **2016**, *326*, 176.

[118] C. Berger, E. Bucher, C. Gspan, W. Sitte, *J. Solid State Chem.* **2019**, *273*, 92.

[119] C. Berger, E. Bucher, A. Windischbacher, A. D. Boese, W. Sitte, *J. Solid State Chem.* **2018**, *259*, 57.

[120] Y. Yamaguchi, I. Kagomiya, S. Minami, H. Shimada, H. Sumi, Y. Ogura, Y. Mizutani, *J. Power Sources* **2020**, *448*, 227426.

[121] R. K. Sharma, M. Burriel, L. Dessemond, J.-M. Bassat, E. Djurado, *J. Power Sources* **2016**, *325*, 337.

[122] R. K. Sharma, M. Burriel, L. Dessemond, V. Martin, J.-M. Bassat, E. Djurado, *J. Power Sources* **2016**, *316*, 17.

[123] R. K. Sharma, S.-K. Cheah, M. Burriel, L. Dessemond, J.-M. Bassat, E. Djurado, *J. Mater. Chem. A* **2017**, *5*, 1120.

[124] V. Vibhu, A. Rougier, C. Nicollet, A. Flura, S. Fourcade, N. Penin, J.-C. Grenier, J.-M. Bassat, *J. Power Sources* **2016**, *317*, 184.

[125] S. Joo, J. Kim, J. Shin, T.-H. Lim, G. Kim, *J. Electrochem. Soc.* **2016**, *163*, F1489.

[126] J. Sun, X. Liu, F. Han, L. Zhu, H. Bi, H. Wang, S. Yu, L. Pei, *Solid State Ion.* **2016**, *288*, 54.

[127] V. Dusastre, J. A. Kilner, *Solid State Ion.* **1999**, *126*, 163.

[128] H. J. Hwang, J.-W. Moon, S. Lee, E. A. Lee, *J. Power Sources* **2005**, *145*, 243.

[129] J. Nielsen, T. Jacobsen, M. Wandel, *Electrochim. Acta* **2011**, *56*, 7963.

[130] E. Perry Murray, M. J. Sever, S. A. Barnett, *Solid State Ion.* **2002**, *148*, 27.

[131] European Commission, European Green Deal, **2019**, https://ec.europa.eu/info/strategy/priorities-2019-2024/european-green-deal_en (accessed: March 2020).

[132] European Commission, 2030 climate & energy framework, **2019**, https://ec.europa.eu/clima/policies/strategies/2030_en (accessed: March 2020).

[133] S. Foit, L. Dittrich, T. Duyster, I. Vinke, R.-A. Eichel, L. G. J. de Haart, *Processes* **2020**, *8*, 1390.

[134] M. S. Khan, X. Xu, J. Zhao, R. Knibbe, Z. Zhu, *J. Power Sources* **2017**, *359*, 104.

[135] A. Hauch, K. Brodersen, M. Chen, C. Graves, S. H. Jensen, P. S. Jørgensen, P. V. Hendriksen, M. B. Mogensen, S. Ovtar, X. Sun, *ECS Trans.* **2017**, *75*, 3.

[136] R. Knibbe, M. L. Traulsen, A. Hauch, S. D. Ebbesen, M. Mogensen, *J. Electrochem. Soc.* **2010**, *157*, B1209.

[137] V. Vibhu, S. Yildiz, I. C. Vinke, R.-A. Eichel, J.-M. Bassat, L. G. J. de Haart, *J. Electrochem. Soc.* **2019**, *166*, F102.

[138] M. Liu, M. G. Millan-Agorio, P. V. Aravind, N. P. Brandon, *J. Electrochem. Soc.* **2011**, *158*, B1310.

[139] N. Bogolowski, B. Iwanschitz, J.-F. Drillet, *Fuel Cells* **2015**, *15*, 711.

[140] H. Jeong, *Coupling a Solid Oxide Fuel Cell with a Biomass Gasifier: Degradation Mechanisms and Alternative Anode Materials*, Vol. 460, Forschungszentrum, Zentralbibliothek, Jülich **2019**.

[141] M. Miyake, S. Matsumoto, M. Iwami, S. Nishimoto, Y. Kameshima, *Int. J. Hydrog. Energy* **2016**, *41*, 13625.

[142] M. Miyake, M. Iwami, M. Takeuchi, S. Nishimoto, Y. Kameshima, *J. Power Sources* **2018**, *390*, 181.

[143] M. B. Mogensen, A. Hauch, X. Sun, M. Chen, Y. Tao, S. D. Ebbesen, K. V. Hansen, P. V. Hendriksen, *Fuel Cells* **2017**, *17*, 434.

[144] M. P. Hoerlein, M. Riegraf, R. Costa, G. Schiller, K. A. Friedrich, *Electrochim. Acta* **2018**, *276*, 162.

[145] Q. Fang, C. E. Frey, N. H. Menzler, L. Blum, *J. Electrochem. Soc.* **2018**, *165*, F38.

[146] C. E. Frey, Q. Fang, D. Sebold, L. Blum, N. H. Menzler, *J. Electrochem. Soc.* **2018**, *165*, F357.

[147] A. Hauch, K. Brodersen, M. Chen, M. B. Mogensen, *Solid State Ion.* **2016**, *293*, 27.

[148] G. Rinaldi, A. Nakajo, P. Caliandro, L. Navratilova, J. Van herle, *ECS Trans.* **2019**, *91*, 641.

[149] Z. Jiao, N. Shikazono, *J. Power Sources* **2018**, *396*, 119.

[150] M. Trini, A. Hauch, S. De Angelis, X. Tong, P. V. Hendriksen, M. Chen, *J. Power Sources* **2020**, *450*, 227599.

[151] N. H. Menzler, D. Sebold, Y. J. Sohn, S. Zischke, *J. Power Sources* **2020**, *478*, 228770.

[152] K. D. Kreuer, *Annu. Rev. Mater. Res.* **2003**, *33*, 333.

[153] E. Fabbri, D. Pergolesi, E. Traversa, *Chem. Soc. Rev.* **2010**, *39*, 4355.

[154] G. Taillades, P. Pers, V. Mao, M. Taillades, *Int. J. Hydrog. Energy* **2016**, *41*, 12330.

[155] L. Yang, S. Wang, K. Blinn, M. Liu, Z. Liu, Z. Cheng, M. Liu, *Science* **2009**, *326*, 126.

[156] C. Duan, J. Tong, M. Shang, S. Nikodemski, M. Sanders, S. Ricote, A. Almansoori, R. O'Hayre, *Science* **2015**, *349*, 1321.

[157] H. An, H.-W. Lee, B.-K. Kim, J.-W. Son, K. J. Yoon, H. Kim, D. Shin, H.-I. Ji, J.-H. Lee, *Nat. Energy* **2018**, *3*, 870.

[158] N. H. Menzler, W. Schafbauer, R. Mücke, R. Kauert, O. Büchler, H. P. Buchkremer, D. Stöver, in *Ceramic Engineering and Science Proc.*, Vol. 32, 4th ed., **2011**, pp. 149.

[159] R. Mücke, N. H. Menzler, H. P. Buchkremer, D. Stöver, *J. Am. Ceram. Soc.* **2009**, *92*, S95.

[160] E. Forster, D. van Holt, M. E. Ivanova, S. Baumann, W. A. Meulenberg, M. Müller, *J. Eur. Ceram. Soc.* **2016**, *36*, 3457.

[161] R. Haugsrud, *Solid State Ion.* **2007**, *178*, 555.

[162] D. van Holt, E. Forster, M. E. Ivanova, W. A. Meulenberg, M. Müller, S. Baumann, R. Vaßen, *J. Eur. Ceram. Soc.* **2014**, *34*, 2381.

[163] K. Leonard, Y. Okuyama, Y. Takamura, Y.-S. Lee, K. Miyazaki, M. E. Ivanova, W. A. Meulenberg, H. Matsumoto, *J. Mater. Chem. A* **2018**, *6*, 19113.

2001062 (16 of 18)

[164] M. Marrony, *Proton-Conducting Ceramics: From Fundamentals to Applied Research*, CRC Press, Boca Raton, FL, USA **2016**.

[165] H. Ding, N. P. Sullivan, S. Ricote, *Solid State Ion.* **2017**, *306*, 97.

[166] E. Fabbri, S. Licoccia, E. Traversa, E. D. Wachsman, *Fuel Cells* **2009**, *9*, 128.

[167] M. E. Ivanova, S. Escolástico, M. Balaguer, J. Palisaitis, Y. J. Sohn, W. A. Meulenberg, O. Guillon, J. Mayer, J. M. Serra, *Sci. Rep.* **2016**, *6*, 34773.

[168] L. Yang, Z. Liu, S. Wang, Y. Choi, C. Zuo, M. Liu, *J. Power Sources* **2010**, *195*, 471.

[169] D. Han, Y. Okumura, Y. Nose, T. Uda, *Solid State Ion.* **2010**, *181*, 1601.

[170] S. Choi, C. J. Kucharczyk, Y. Liang, X. Zhang, I. Takeuchi, H.-I. Ji, S. M. Haile, *Nat. Energy* **2018**, *3*, 202.

[171] L. Fan, P.-C. Su, *J. Power Sources* **2016**, *306*, 369.

[172] H. Téllez Lozano, J. Druce, S. J. Cooper, J. A. Kilner, *Sci. Technol. Adv. Mater.* **2017**, *18*, 977.

[173] J. Dailly, M. Marrony, G. Taillades, M. Taillades-Jacquin, A. Grimaud, F. Mauvy, E. Louradour, J. Salmi, *J. Power Sources* **2014**, *255*, 302.

[174] R. Strandbakke, V. A. Cherepanov, A. Y. Zuev, D. S. Tsvetkov, C. Argirusis, G. Sourkouni, S. Prünte, T. Norby, *Solid State Ion.* **2015**, *278*, 120.

[175] R. Strandbakke, E. Vøllestad, S. A. Robinson, M.-L. Fontaine, T. Norby, *J. Electrochem. Soc.* **2017**, *164*, F196.

[176] G. Li, H. Jin, Y. Cui, L. Gui, B. He, L. Zhao, *J. Power Sources* **2017**, *341*, 192.

[177] S. Wang, J. Shen, Z. Zhu, Z. Wang, Y. Cao, X. Guan, Y. Wang, Z. Wei, M. Chen, *J. Power Sources* **2018**, *387*, 24.

[178] L. Zhao, G. Li, K. Chen, Y. Ling, Y. Cui, L. Gui, B. He, *J. Power Sources* **2016**, *333*, 24.

[179] C. Duan, R. Kee, H. Zhu, N. Sullivan, L. Zhu, L. Bian, D. Jennings, R. O'Hayre, *Nat. Energy* **2019**, *4*, 230.

[180] S. Choi, T. C. Davenport, S. M. Haile, *Energy Environ. Sci.* **2019**, *12*, 206.

[181] J. Kim, A. Jun, O. Gwon, S. Yoo, M. Liu, J. Shin, T.-H. Lim, G. Kim, *Nano Energy* **2018**, *44*, 121.

[182] W. Wu, H. Ding, Y. Zhang, Y. Ding, P. Katiyar, P. K. Majumdar, T. He, D. Ding, *Adv. Sci.* **2018**, *5*, 1800360.

[183] R. Wang, F. Jin, L. Ta, T. He, *Solid State Ion.* **2016**, *288*, 32.

[184] W. Zhang, J. Meng, X. Zhang, L. Zhang, X. Liu, J. Meng, *Solid State Ion.* **2018**, *316*, 20.

[185] A. S. Painter, Y.-L. Huang, E. D. Wachsman, *J. Power Sources* **2017**, *360*, 391.

[186] J. Hou, L. Bi, J. Qian, Z. Gong, Z. Zhu, W. Liu, *J. Power Sources* **2016**, *301*, 306.

[187] Z. Zhang, Y. Zhu, Y. Zhong, W. Zhou, Z. Shao, *Adv. Energy Mater.* **2017**, *7*, 1700242.

[188] W. Sun, P. Li, C. Xu, L. Dong, J. Qiao, Z. Wang, D. Rooney, K. Sun, *J. Power Sources* **2017**, *343*, 237.

[189] J. Nielsen, Å. H. Persson, B. R. Sudireddy, J. T. S. Irvine, K. Thydén, *J. Power Sources* **2017**, *372*, 99.

[190] Q. Ma, S. Dierickx, V. Vibhu, D. Sebold, L. G. J. de Haart, A. Weber, O. Guillon, N. H. Menzler, *J. Electrochem. Soc.* **2020**, *167*, 084522.

[191] S. Pang, W. Wang, Y. Su, X. Shen, Y. Wang, K. Xu, C. Chen, *J. Electrochem. Soc.* **2017**, *164*, F775.

[192] X. Meng, Y. Shen, M. Xie, Y. Yin, N. Yang, Z.-F. Ma, J. C. Diniz da Costa, S. Liu, *J. Power Sources* **2016**, *306*, 226.

[193] F. Dong, M. Ni, W. He, Y. Chen, G. Yang, D. Chen, Z. Shao, *J. Power Sources* **2016**, *326*, 459.

[194] L. Zhang, S. Li, T. Xia, L. Sun, L. Huo, H. Zhao, *Int. J. Hydrog. Energy* **2018**, *43*, 3761.

[195] A. Chrzan, S. Ovtar, P. Jasinski, M. Chen, A. Hauch, *J. Power Sources* **2017**, *353*, 67.

[196] Y.-F. Bu, Q. Zhong, D.-C. Chen, Y. Chen, S. Y. Lai, T. Wei, H.-B. Sun, D. Ding, M. Liu, *J. Power Sources* **2016**, *319*, 178.

[197] D. Y. Jang, M. Kim, J. W. Kim, K. Bae, J.-W. Son, M. V. F. Schlupp, J. H. Shim, *J. Electrochem. Soc.* **2017**, *164*, F484.

[198] H. Shimada, T. Yamaguchi, T. Suzuki, H. Sumi, K. Hamamoto, Y. Fujishiro, *J. Power Sources* **2016**, *302*, 308.

[199] G. M. Rupp, A. Schmid, A. Nenning, J. Fleig, *J. Electrochem. Soc.* **2016**, *163*, F564.

[200] H. Qi, Z. Zhao, B. Tu, M. Cheng, *J. Power Sources* **2020**, *455*, 227971.

[201] S. Ovtar, M. Chen, A. J. Samson, R. Kiebach, *Solid State Ion.* **2017**, *304*, 51.

[202] H.-S. Noh, K. J. Yoon, B.-K. Kim, H.-J. Je, H.-W. Lee, J.-H. Lee, J.-W. Son, *J. Power Sources* **2014**, *247*, 105.

[203] R. T. Leah, A. Bone, E. Hammer, A. Selcuk, M. Rahman, A. Clare, L. Rees, N. Lawrence, A. Ballard, T. Domanski, S. Mukerjee, M. Selby, *ECS Trans.* **2017**, *78*, 2005.

[204] M. Haydn, C. Bischof, D. Udomsilp, A. K. Opitz, G. Bimashofer, W. Schafbauer, M. Brandner, M. Bram, *ECS Trans.* **2017**, *78*, 1993.

[205] E. Dogdibegovic, R. Wang, G. Y. Lau, M. C. Tucker, *J. Power Sources* **2019**, *410–411*, 91.

[206] S. Zhen, W. Sun, P. Li, G. Tang, D. Rooney, K. Sun, X. Ma, *J. Power Sources* **2016**, *315*, 140.

[207] L. Shao, P. Wang, Q. Zhang, L. Fan, N. Zhang, K. Sun, *J. Power Sources* **2017**, *343*, 268.

[208] L. Ding, L. Wang, D. Ding, S. Zhang, X. Ding, G. Yuan, *J. Power Sources* **2017**, *354*, 26.

[209] K.-J. Pan, A. M. Hussain, E. D. Wachsman, *J. Power Sources* **2017**, *347*, 277.

[210] L. dos Santos-Gómez, J. M. Porras-Vázquez, E. R. Losilla, F. Martín, J. R. Ramos-Barrado, D. Marrero-López, *J. Power Sources* **2017**, *347*, 178.

[211] T. Hong, K. Brinkman, C. Xia, *J. Power Sources* **2016**, *329*, 281.

[212] Ö. Çelikbilek, D. Jauffrès, E. Siebert, L. Dessemond, M. Burriel, C. L. Martin, E. Djurado, *J. Power Sources* **2016**, *333*, 72.

[213] T. Ishihara, S. Wang, K.-T. Wu, *Solid State Ion.* **2017**, *299*, 60.

[214] C. Zhu, L. Hou, S. Li, L. Gan, K. Xie, *J. Power Sources* **2017**, *363*, 177.

[215] J. Yan, Z. Zhao, L. Shang, D. Ou, M. Cheng, *J. Power Sources* **2016**, *319*, 124.

[216] H. Zheng, Y. Tian, L. Zhang, B. Chi, J. Pu, J. Lian, *J. Power Sources* **2018**, *383*, 93.

[217] X. Tong, S. Ovtar, K. Brodersen, P. V. Hendriksen, M. Chen, *J. Power Sources* **2020**, *451*, 227742.

[218] E. Dogdibegovic, F. Shen, R. Wang, I. Robinson, G. Y. Lau, M. C. Tucker, *ECS Trans.* **2019**, *91*, 877.

[219] L. Gui, Y. Ling, G. Li, Z. Wang, Y. Wan, R. Wang, B. He, L. Zhao, *J. Power Sources* **2016**, *301*, 369.

[220] Z. Chen, J. Wang, D. Huan, S. Sun, G. Wang, Z. Fu, W. Zhang, X. Zheng, H. Pan, R. Peng, Y. Lu, *J. Power Sources* **2017**, *371*, 41.

[221] A. R. Hanifi, N. K. Sandhu, T. H. Etsell, J.-L. Luo, P. Sarkar, *J. Power Sources* **2017**, *341*, 264.

[222] Y. Wan, B. He, R. Wang, Y. Ling, L. Zhao, *J. Power Sources* **2017**, *347*, 14.

David Udomsilp is a research associate at the Institute of Energy and Climate Research, Materials Synthesis and Processing (IEK-1) at Forschungszentrum Jülich. He received a M.Sc. degree in materials engineering from RWTH Aachen University and holds a Ph.D. degree in mechanical engineering. His scientific work includes processing and characterization of functional ceramics for solid oxide cells. In addition to the work on metal-supported and ASCs, he currently focuses on development activities required for industrialization of solid oxide cells.

Christian Lenser is a staff scientist at the Institute of Energy and Climate Research – Materials Synthesis and Processing (IEK-1) at Forschungszentrum Jülich. He studied Materials Science at RWTH Aachen University and Technical University of Munich, graduating with his M.Sc. degree, in 2009. He obtained his Ph.D. degree at RWTH Aachen University, in 2013. After spending a year at Massachusetts Institute of Technology (MIT), he joined the Solid Oxide Cells department at IEK-1, in 2015. His research interests are focused on the development and processing of components for SOCs operating at low temperature, as well as for high-temperature electrolysis applications.

Olivier Guillon is a materials scientist and became director at the Institute of Energy and Climate Research—Materials Synthesis and Processing (IEK-1, Forschungszentrum Jülich) and professor at the RWTH Aachen University, in 2014. He is the spokesperson of the research program "Materials and Technologies for the Energy Transition" within the Helmholtz Association and works on ceramic materials and components for solid oxide fuel and electrolysis cells, gas separation membranes, solid-state batteries, and high-temperature applications.

Norbert H. Menzler studied materials science at the University of Erlangen-Nuremberg from which he got his Diploma and his Ph.D. degrees. Afterwards, he acted as a managing director of a Bavarian research network. In 2000, he joined the Forschungszentrum Jülich working now on Solid Oxide Cells. His specializations are the cell materials, their processing, and the post-test analysis of operated stacks. Since 2016, he has been the head of the Solid Oxide Cell department of the Institute of Energy and Climate Research (IEK-1: Materials Synthesis and Processing).